Akkari, M., Duan L. "Nonlinear Analysis of Bridge Structures."
Bridge Engineering Handbook.
Ed. Wai-Fah Chen and Lian Duan
Boca Raton: CRC Press, 2000

36

Nonlinear Analysis of Bridge Structures

Mohammed Akkari
California Department of Transportation

Lian Duan
California Department of Transportation

36.1 Introduction

In recent years, nonlinear bridge analysis has gained a greater momentum because of the need to assess inelastic structural behavior under seismic loads. Common seismic design philosophies for ordinary bridges allow some degree of damage without collapse. To control and evaluate damage, a postelastic nonlinear analysis is required. A nonlinear analysis is complex and involves many simplifying assumptions. Engineers must be familiar with those complexities and assumptions to design bridges that are safe and economical.

Many factors contribute to the nonlinear behavior of a bridge. These include factors such as material inelasticity, geometric or second-order effects, nonlinear soil–foundation–structure inter-action, gap opening and closing at hinges and abutment locations, time-dependent effects due to concrete creep and shrinkage, etc. The subject of nonlinear analysis is extremely broad and cannot be covered in detail in this single chapter. Only material and geometric nonlinearities as well as
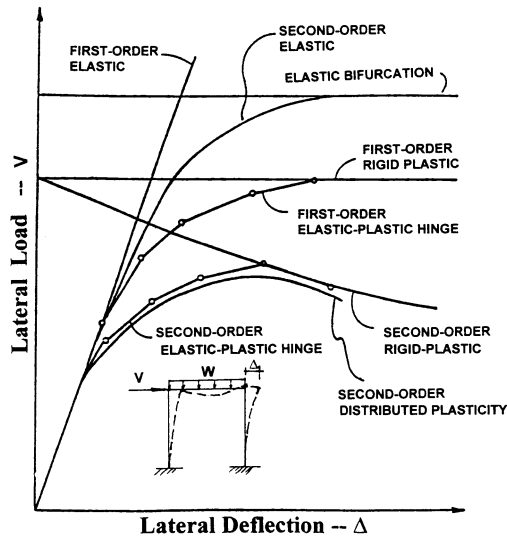
FIGURE 36.1   Lateral load–displacement curves of a frame.

some of the basic formulations of nonlinear static analysis with their practical applications to seismic bridge design will be presented here. The reader is referred to the many excellent papers, reports, and books [1-8] that cover this type of analysis in more detail.

In this chapter, some general guidelines for nonlinear static analysis are presented. These are followed by discussion of the formulations of geometric and material nonlinearities for section and frame analysis. Two examples are given to illustrate the applications of static nonlinear push-over analysis in bridge seismic design.

36.2   Analysis Classification and General Guidelines

Engineers use structural analysis as a fundamental tool to make design decisions. It is important that engineers have access to several different analysis tools and understand their development assumptions and limitations. Such an understanding is essential to select the proper analysis tool to achieve the design objectives.

Figure 36.1 shows lateral load vs. displacement curves of a frame using several structural analysis methods. Table 36.1 summarizes basic assumptions of those methods. It can be seen from Figure 36.1 that the first-order elastic analysis gives a straight line and no failure load. A first-order inelastic analysis predicts the maximum plastic load-carrying capacity on the basis of the undeformed geometry. A second-order elastic analysis follows an elastic buckling process. A second-order inelastic analysis traces load–deflection curves more accurately.

36.2.1   Classifications

Structural analysis methods can be classified on the basis of different formulations of equilibrium, the constitutive and compatibility equations as discussed below.

Classification Based on Equilibrium and Compatibility Formulations

First-order analysis: An analysis in which equilibrium is formulated with respect to the undeformed (or original) geometry of the structure. It is based on small strain and small displacement theory.

TABLE 36.1   Structural Analysis Methods

| Methods		Features		
		Constitutive Relationship	Equilibrium Formulation	Geometric Compatibility
First-order	Elastic Rigid–plastic Elastic–plastic hinge Distributed plasticity	Elastic Rigid plastic Elastic perfectly plastic Inelastic	Original undeformed geometry	Small strain and small displacement
Second-order	Elastic Rigid–plastic Elastic–plastic hinge Distributed plasticity	Elastic Rigid plastic Elastic perfectly plastic Inelastic	Deformed structural geometry (P-Δ and P-δ)	Small strain and moderate rotation (displacement may be large)
True large displacement	Elastic Inelastic	Elastic Inelastic	Deformed structural geometry	Large strain and large deformation
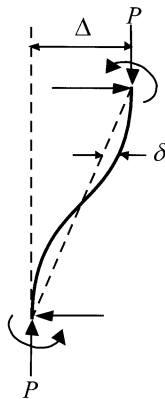
FIGURE 36.2   Second–order effects.

Second-order analysis: An analysis in which equilibrium is formulated with respect to the deformed geometry of the structure. A second-order analysis usually accounts for the P-Δ effect (influence of axial force acting through displacement associated with member chord rotation) and the P-δ effect (influence of axial force acting through displacement associated with member flexural curvature) (see Figure 36.2). It is based on small strain and small member deformation, but moderate rotations and large displacement theory.

True large deformation analysis: An analysis for which large strain and large deformations are taken into account.

Classification Based on Constitutive Formulation

Elastic analysis: An analysis in which elastic constitutive equations are formulated.

Inelastic analysis: An analysis in which inelastic constitutive equations are formulated.

Rigid–plastic analysis: An analysis in which elastic rigid–plastic constitutive equations are formulated.

Elastic–plastic hinge analysis: An analysis in which material inelasticity is taken into account by using concentrated "zero-length" plastic hinges.

Distributed plasticity analysis: An analysis in which the spread of plasticity through the cross sections and along the length of the members are modeled explicitly.

Classification Based on Mathematical Formulation

Linear analysis: An analysis in which equilibrium, compatibility, and constitutive equations are linear.

Nonlinear analysis: An analysis in which some or all of the equilibrium, compatibility, and constitutive equations are nonlinear.

36.2.4 General Guidelines

The following guidelines may be useful in analysis type selection:

- A first-order analysis may be adequate for short- to medium-span bridges. A second-order analysis should always be encouraged for long-span, tall, and slender bridges. A true large displacement analysis is generally unnecessary for bridge structures.
- An elastic analysis is sufficient for strength-based design. Inelastic analyses should be used for displacement-based design.
- The bowing effect (effect of flexural bending on member's axial deformation), the Wagner effect (effect of bending moments and axial forces acting through displacements associated with the member twisting), and shear effects on solid-webbed members can be ignored for most of bridge structures.
- For steel nonlinearity, yielding must be taken into account. Strain hardening and fracture may be considered. For concrete nonlinearity, a complete strain–stress relationship (in compression up to the ultimate strain) should be used. Concrete tension strength can be neglected.
- Other nonlinearities, most importantly, soil–foundation–structural interaction, seismic response modification devices (dampers and seismic isolations), connection flexibility, gap close and opening should be carefully considered.

36.3 Geometric Nonlinearity Formulation

Geometric nonlinearities can be considered in the formulation of member stiffness matrices. The general force–displacement relationship for the prismatic member as shown in Figure 36.3 can be expressed as follows:

$$\{F\} = [K]\{D\} \tag{36.1}$$

where $\{F\}$ and $\{D\}$ are force and displacement vectors and $[K]$ is stiffness matrix.

For a two-dimensional member as shown in Figure 36.3a

$$\{F\} = \left\{P_{1a},\ F_{2a},\ M_{3a},\ P_{1b}, F_{2b}, M_{3b}\right\}^{T} \tag{36.2}$$

$$\{D\} = \left\{u_{1a},\ u_{2a},\ \theta_{3a},\ u_{1b}, u_{2b}, \theta_{3b}\right\}^{T} \tag{36.3}$$

For a three-dimensional member as shown in Figure 36.3b

$$\{F\} = \{P_{1a}, F_{2a}, F_{3a}, M_{1a}, M_{2a}, M_{3a}, P_{1b}, F_{2b}, F_{3b}, M_{1b}, M_{2b}, M_{3b}\}^{I} \tag{36.4}$$

$$\{D\} = \{u_{1a}, u_{2a}, u_{3a}, \theta_{1a}, \theta_{2a}, \theta_{3a}, u_{1b}, u_{2b}, u_{3b}, \theta_{1b}, \theta_{2b}, \theta_{3b}\}^{I} \tag{36.5}$$
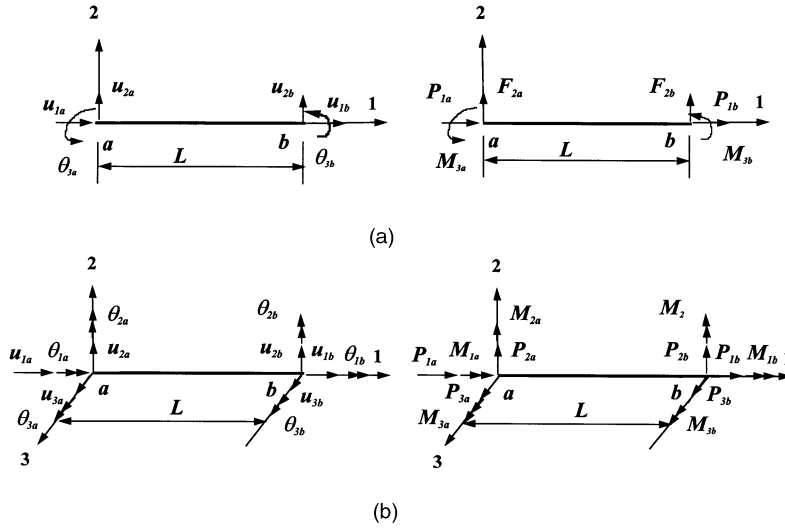
FIGURE 36.3 Degrees of freedom and nodal forces for a framed member. (a) Two-dimensional and (b) three-dimensional members.

Two sets of formulations of stability function-based and finite-element-based stiffness matrices are presented in the following section.

36.3.1 Two-Dimensional Members

For a two-dimensional prismatic member as shown in Figure 36.3a, the stability function-based stiffness matrix [9] is as follows:

$$
[K] = \begin{vmatrix}
\dfrac{AE}{L} & 0 & 0 & -\dfrac{AE}{L} & 0 & 0 \\[2mm]
 & \dfrac{12EI}{L^3}\phi_1 & \dfrac{-6EI}{L^2}\phi_2 & 0 & \dfrac{-12EI}{L^3}\phi & \dfrac{-6EI}{L^2}\phi_2 \\[2mm]
 & & 4\phi_3 & 0 & \dfrac{6EI}{L^2}\phi_2 & 2\phi_4 \\[2mm]
 & & & \dfrac{AE}{L} & 0 & 0 \\[2mm]
 & & & & \dfrac{12EI}{L^3}\phi & \dfrac{6EI}{L^2}\phi_2 \\[2mm]
 & & & & & 4\phi_3
\end{vmatrix}
\tag{36.6}
$$

where A is cross section area; E is the material modulus of elasticity; L is the member length; ϕ_1, ϕ_2, ϕ_3, and ϕ_4 can be expressed by stability equations and are listed in Table 36.2. Alternatively, ϕ_i functions can also be expressed in the power series derived from the analytical solutions [10] as listed in Table 36.3.

Assuming polynomial displacement functions, the finite-element-based stiffness matrix [11,12] has the following form:

$$
[K] = [K_e] + [K_g]
\tag{36.7}
$$

where $[K_e]$ is the first-order conventional linear elastic stiffness matrix and $[K_g]$ is the geometric stiffness matrix which considers the effects of axial load on the bending stiffness of a member.

TABLE 36.2   Stability Function-Based ϕ_i Equations for Two-Dimensional Member

ϕ	Axial Load P		
	Compression	Zero	Tension
ϕ_1	$\dfrac{(kL)^3 \sin kL}{12\phi_c}$	1	$\dfrac{(kL)^3 \sinh kL}{12\phi_t}$
ϕ_2	$\dfrac{(kL)^2(1-\cos kL)}{6\phi_c}$	1	$\dfrac{(kL)^2(\cosh kL - 1)}{6\phi_t}$
ϕ_3	$\dfrac{(kL)(\sin kL - kL\cos kL)}{4\phi_c}$	1	$\dfrac{(kL)(kL\cosh kL - \sinh kL)}{4\phi_t}$
ϕ_4	$\dfrac{(kL)(kL - \sin kL)}{2\phi_c}$	1	$\dfrac{(kL)(\sin kL - kL)}{2\phi_t}$

Note: $\phi_c = 2 - 2\cos kL - kL\sin kL$; $\phi_t = 2 - 2\cosh kL - kL\sinh kL$; $k = \sqrt{P/EI}$.

TABLE 36.3   Power Series Expression of ϕ_i Equations

ϕ_1	$\dfrac{1 + \sum\limits_{n=1}^{\infty} \dfrac{1}{(2n+1)!}\left[\mp(kL)^2\right]^n}{12\phi}$
ϕ_2	$\dfrac{\dfrac{1}{2} + \sum\limits_{n=1}^{\infty} \dfrac{1}{(2n+2)!}\left[\mp(kL)^2\right]^n}{6\phi}$
ϕ_3	$\dfrac{\dfrac{1}{3} + \sum\limits_{n=1}^{\infty} \dfrac{2(n+1)}{(2n+3)!}\left[\mp(kL)^2\right]^n}{4\phi}$
ϕ_4	$\dfrac{\dfrac{1}{6} + \sum\limits_{n=1}^{\infty} \dfrac{1}{(2n+3)!}\left[\mp(kL)^2\right]^n}{2\phi}$
ϕ	$\dfrac{1}{12} + \sum\limits_{n=1}^{\infty} \dfrac{2(n+1)}{(2n+4)!}\left[\mp(kL)^2\right]^n$

Note: minus sign = compression; plus sign = tension.

$$[\boldsymbol{K}] = \begin{vmatrix} \dfrac{AE}{L} & 0 & 0 & -\dfrac{AE}{L} & 0 & 0 \\[2mm] & \dfrac{12EI}{L^3} & \dfrac{-6EI}{L^2} & 0 & \dfrac{-12EI}{L^3} & \dfrac{-6EI}{L^2} \\[2mm] & & 4 & 0 & \dfrac{6EI}{L^2} & 2 \\[2mm] & & & \dfrac{AE}{L} & 0 & 0 \\[2mm] & \text{sym} & & & \dfrac{12EI}{L^3} & \dfrac{6EI}{L^2} \\[2mm] & & & & & 4 \end{vmatrix} \qquad (36.8)$$

$$
[K_g] = \mathrm{m}\frac{P}{L}
\begin{bmatrix}
0 & 0 & 0 & 0 & 0 & 0 \\
 & \dfrac{6}{5} & \dfrac{-L}{10} & 0 & \dfrac{-6}{5} & \dfrac{-L}{10} \\
 & & \dfrac{2L^2}{15} & 0 & \dfrac{L}{10} & -\dfrac{L^2}{30} \\
 & & & 0 & 0 & 0 \\
 & \text{sym.} & & & \dfrac{6}{5} & \dfrac{L}{10} \\
 & & & & & \dfrac{2L^2}{15}
\end{bmatrix}
\tag{36.9}
$$

It is noted [13] that Eqs. (36.8) and (36.9) exactly coincide with the stability function-based stiffness matrix when taken only the first two terms of the Taylor series expansion in Eq. (36.6).

36.3.2 Three-Dimensional Members

For a three-dimensional frame member as shown in Figure 36.3b, the stability function-based stiffness matrix has the following form [14]:

$$
[K] =
\begin{bmatrix}
\phi_{s1} & 0 & 0 & 0 & 0 & 0 & -\phi_{s1} & 0 & 0 & 0 & 0 & 0 \\
 & \phi_{s7} & 0 & 0 & 0 & \phi_{s6} & 0 & -\phi_{s7} & 0 & 0 & 0 & \phi_{s6} \\
 & & \phi_{s9} & 0 & -\phi_{s8} & 0 & 0 & 0 & -\phi_{s9} & 0 & -\phi_{s8} & 0 \\
 & & & \dfrac{GJ}{L} & 0 & 0 & 0 & 0 & 0 & -\dfrac{GJ}{L} & 0 & 0 \\
 & & & & \phi_{s4} & 0 & 0 & 0 & \phi_{s8} & 0 & \phi_{s5} & 0 \\
 & & & & & \phi_{s2} & 0 & -\phi_{s6} & 0 & 0 & 0 & \phi_{s3} \\
 & & & & & & \phi_{s1} & 0 & 0 & 0 & 0 & 0 \\
 & & & & & & & \phi_{s7} & 0 & 0 & 0 & -\phi_{s6} \\
 & \text{Sym.} & & & & & & & \phi_{s9} & 0 & \phi_{s8} & 0 \\
 & & & & & & & & & \dfrac{GJ}{L} & 0 & 0 \\
 & & & & & & & & & & \phi_{s4} & 0 \\
 & & & & & & & & & & & \phi_{s2}
\end{bmatrix}
\tag{36.10}
$$

where G is shear modulus of elasticity; J is torsional constant; ϕ_{s1} to ϕ_{s9} are expressed by stability equations and listed in Table 36.4.

Finite-element-based stiffness matrix has the form [15]:

$$
[K_e] =
\begin{bmatrix}
\phi_{e1} & 0 & 0 & 0 & 0 & 0 & -\phi_{e1} & 0 & 0 & 0 & 0 & 0 \\
 & \phi_{e7} & 0 & 0 & 0 & \phi_{e6} & 0 & -\phi_{e7} & 0 & 0 & 0 & \phi_{e6} \\
 & & \phi_{e9} & 0 & -\phi_{e8} & 0 & 0 & 0 & -\phi_{e9} & 0 & -\phi_{e8} & 0 \\
 & & & \dfrac{GJ}{L} & 0 & 0 & 0 & 0 & 0 & -\dfrac{GJ}{L} & 0 & 0 \\
 & & & & \phi_{e4} & 0 & 0 & 0 & -\phi_{e8} & 0 & \phi_{e5} & 0 \\
 & & & & & \phi_{e2} & 0 & -\phi_{e6} & 0 & 0 & 0 & \phi_{e3} \\
 & & & & & & \phi_{e1} & 0 & 0 & 0 & 0 & 0 \\
 & & & & & & & \phi_{e7} & 0 & 0 & \mathbf{0} & -\phi_{e6} \\
 & \text{Sym.} & & & & & & & \phi_{e9} & 0 & \phi_{e8} & 0 \\
 & & & & & & & & & \dfrac{GJ}{L} & 0 & 0 \\
 & & & & & & & & & & \phi_{e4} & 0 \\
 & & & & & & & & & & & \phi_{e2}
\end{bmatrix}
\tag{36.11}
$$

TABLE 36.4   Stability Function-Based ϕ_{si} for Three-Dimensional Member

ϕ_{si}		Stability Functions S_i	
		Compression	Tension
$\phi_{s1} = S_1 \dfrac{EA}{L}$	S_1	$\dfrac{1}{1 - \dfrac{EA}{4P^3 L^2}\left[H_y + H_z\right]}$	$\dfrac{1}{1 - \dfrac{EA}{4P^3 L^2}\left[H'_y + H'_z\right]}$
$\phi_{s2} = S_2 \dfrac{(4+\phi_y)EI_Z}{(1+\phi_y)L}$	S_2	$\dfrac{(\alpha L)(\sin\alpha L - \alpha L\cos\alpha L)}{4\phi_\alpha}$	$\dfrac{(\alpha L)(\alpha L\cosh\alpha L - \sinh\alpha L)}{4\phi_\alpha}$
$\phi_{s3} = S_2 \dfrac{(2-\phi_y)EI_Z}{(1+\phi_y)L}$	S_3	$\dfrac{(\alpha L)(\alpha L - \sin\alpha L)}{2\phi_\alpha}$	$\dfrac{(\alpha L)(\sinh\alpha L - \alpha L)}{2\phi_\alpha}$
$\phi_{s4} = S_4 \dfrac{(4+\phi_z)EI_y}{(1+\phi_z)L}$	S_4	$\dfrac{(\beta L)(\sin\beta L - \beta L\cos\beta L)}{4\phi_\beta}$	$\dfrac{(\beta L)(\beta L\cosh\beta L - \sinh\beta L)}{4\phi_\beta}$
$\phi_{s5} = S_2 \dfrac{(2-\phi_z)EI_y}{(1+\phi_z)L}$	S_5	$\dfrac{(\beta L)(\beta L - \sin\beta L)}{2\phi_\beta}$	$\dfrac{(\beta L)(\sinh\beta L - \beta L)}{2\phi_\beta}$
$\phi_{s6} = S_6 \dfrac{6EI_Z}{(1+\phi_y)L^2}$	S_6	$\dfrac{(\alpha L)^2(1-\cos\alpha L)}{6\phi_\alpha}$	$\dfrac{(\alpha L)^2(\cosh\alpha L - 1)}{6\phi_\alpha}$
$\phi_{s7} = S_7 \dfrac{12EI_Z}{(1+\phi_y)L^3}$	S_7	$\dfrac{(\alpha L)^3 \sin\alpha L}{12\phi_\alpha}$	$\dfrac{(\alpha L)^3 \sinh\alpha L}{12\phi_\alpha}$
$\phi_{s8} = S_8 \dfrac{6EI_y}{(1+\phi_z)L^2}$	S_8	$\dfrac{(\beta L)^2(1-\cos\beta L)}{6\phi_\beta}$	$\dfrac{(\beta L)^2(\cosh\beta L - 1)}{6\phi_\beta}$
$\phi_{s9} = S_9 \dfrac{12EI_y}{(1+\phi_z)L^3}$	S_9	$\dfrac{(\beta L)^3 \sin\beta L}{12\phi_\beta}$	$\dfrac{(\beta L)^3 \sinh\beta L}{12\phi_\beta}$
$\alpha = \sqrt{P/EI_Z}$	ϕ_α	$2 - 2\cos\alpha L - \alpha L\sin\alpha L$	$2 - 2\cosh\alpha L + \alpha L\sinh\alpha L$
$\beta = \sqrt{P/EI_y}$	ϕ_β	$2 - 2\cos\beta L - \beta L\sin\beta L$	$2 - 2\cosh\beta L + \beta L\sinh\beta L$

$H_y = \beta L(M_{ya}^2 + M_{yb}^2)(\cot\beta L + \beta L\cos ec^2\beta L) - 2(M_{ya} + M_{yb})^2 + 2\beta L M_{ya}M_{yb}(\cos ec\beta L)(1 + \beta L\cot\beta L)$

$H_z = \alpha L(M_{za}^2 + M_{zb}^2)(\cot\alpha L + \alpha L\cos ec^2\alpha L) - 2(M_{za} + M_{zb})^2 + 2\alpha L M_{za}M_{zb}(\cos ec\alpha L)(1 + \alpha L\cot\alpha L)$

$H'_y = \beta L(M_{ya}^2 + M_{yb}^2)(\coth\beta L + \beta L\cos ech^2\beta L) - 2(M_{ya} + M_{yb})^2 + 2\beta L M_{ya}M_{yb}(\cos ech\beta L)(1 + \beta L\coth\beta L)$

$H'_z = \alpha L(M_{za}^2 + M_{zb}^2)(\coth\alpha L + \alpha L\cos ech^2\alpha L) - 2(M_{za} + M_{zb})^2 + 2\alpha L M_{za}M_{zbb}(\cos ech\alpha L)(1 + \alpha L\coth\alpha L)$

$$
[K_g] =
\begin{bmatrix}
\phi_{g1} & \phi_{g10} & -\phi_{g11} & 0 & 0 & 0 & 0 & -\phi_{g10} & \phi_{g11} & 0 & 0 & 0 \\
 & \phi_{g7} & 0 & \phi_{g12} & \phi_{g13} & \phi_{g6} & -\phi_{g10} & -\phi_{g7} & 0 & \phi_{g14} & -\phi_{g13} & \phi_{g6} \\
 & & \phi_{g9} & \phi_{g15} & -\phi_{g6} & \phi_{g13} & \phi_{g11} & 0 & -\phi_{g9} & \phi_{g16} & -\phi_{g6} & -\phi_{g13} \\
 & & & \phi_{g17} & \phi_{g18} & \phi_{g19} & & -\phi_{g12} & -\phi_{g15} & -\phi_{g17} & -\phi_{g20} & \phi_{g21} \\
 & & & & \phi_{g4} & 0 & 0 & -\phi_{g13} & \phi_{g6} & -\phi_{g20} & -\phi_{g5} & \phi_{g13} \\
 & & & & & \phi_{g2} & 0 & -\phi_{g6} & -\phi_{g13} & \phi_{g21} & -\phi_{g13} & -\phi_{g3} \\
 & & & & & & \phi_{g1} & \phi_{g10} & -\phi_{g11} & 0 & 0 & 0 \\
 & & & & & & & \phi_{g7} & 0 & -\phi_{g14} & \phi_{g13} & -\phi_{g6} \\
 & \text{Sym.} & & & & & & & \phi_{g9} & -\phi_{g16} & \phi_{g6} & \phi_{g13} \\
 & & & & & & & & & \phi_{g17} & \phi_{g18} & \phi_{g19} \\
 & & & & & & & & & & \phi_{g4} & 0 \\
 & & & & & & & & & & & \phi_{g2}
\end{bmatrix}
\tag{36.12}
$$

where ϕ_{ei} and ϕ_{gi} are given in Table 36.5.

TABLE 36.5 Elements of Finite-Element-Based Stiffness Matrix

Linear Elastic Matrix	Geometric Nonlinear Matrix

$$\phi_{e1} = \frac{AE}{L} ; \qquad \phi_{e2} = \frac{4EI_z}{L} \qquad\qquad \phi_{g1} = 0 ; \quad \phi_{g2} = \phi_{g4} = \frac{2F_{xb}L}{15} ; \quad \phi_{g3} = \phi_{g5} = \frac{F_{xb}L}{30}$$

$$\phi_{e3} = \frac{2EI_z}{L} \qquad \phi_{e4} = \frac{4EI_y}{L} \qquad\qquad \phi_{g7} = \phi_{g9} = \frac{6F_{xb}}{5L} ; \quad \phi_{g6} = \phi_{g8} = \frac{F_{xb}}{10} ; \quad \phi_{g10} = \frac{M_{za} + M_{zb}}{L^2}$$

$$\phi_{e5} = \frac{2EI_y}{L} ; \quad \phi_{e6} = \frac{6EI_z}{L^2} \qquad\qquad \phi_{g11} = \frac{M_{ya} + M_{yb}}{L^2} ; \quad \phi_{g12} = \frac{M_{ya}}{L} ; \quad \phi_{g13} = \frac{M_{xb}}{L}$$

$$\phi_{e7} = \frac{12EI_Z}{L^3} ; \quad \phi_{e8} = \frac{6EI_y}{L^2} \qquad\qquad \phi_{g14} = \frac{M_{yb}}{L} ; \quad \phi_{g15} = \frac{M_{za}}{L} ; \quad \phi_{g16} = \frac{M_{zb}}{L}$$

$$\phi_{e9} = \frac{12EI_y}{L^3} \qquad\qquad\qquad\qquad \phi_{g17} = \frac{F_{xb}I_p}{AL} ; \quad \phi_{g18} = \frac{M_{zb}}{6} - \frac{M_{za}}{3} ; \quad \phi_{g19} = \frac{M_{ya}}{3} - \frac{M_{yb}}{6}$$

$$\phi_{g20} = \frac{M_{za} + M_{zyb}}{6} ; \quad \phi_{g21} = \frac{M_{ya} + M_{yb}}{6}$$

I_z and I_y are moments of inertia about z–z and y–y axis, respectively; I_p is the polar moment of inertia.

Stiffness matrices considering warping degree of freedom and finite rotations for a thin-walled member were derived by Yang and McGuire [16,17].

In conclusion, both sets of the stiffness matrices have been used successfully when considering geometric nonlinearities (P-Δ and P-δ effects). The stability function-based formulation gives an accurate solution using fewer degrees of freedom when compared with the finite-element method. Its power series expansion (Table 36.3) can be implemented easily without truncation to avoid numerical difficulty.

The finite-element-based formulation produces an approximate solution. It has a simpler form and may require dividing the member into a large number of elements in order to keep the (P/L) term a small quantity to obtain accurate results.

36.4 Material Nonlinearity Formulations

36.4.1 Structural Concrete

Concrete material nonlinearity is incorporated into analysis using a nonlinear stress–strain relationship. Figure 36.4 shows idealized stress–strain curves for unconfined and confined concrete in uniaxial compression. Tests have shown that the confinement provided by closely spaced transverse reinforcement can substantially increase the ultimate concrete compressive stress and strain. The confining steel prevents premature buckling of the longitudinal compression reinforcement and increases the concrete ductility. Extensive research has been made to develop concrete stress–strain relationships [18-25].

36.4.1.1 Compression Stress–Strain Relationship

Unconfined Concrete
A general stress–strain relationship proposed by Hognestad [18] is widely used for plain concrete or reinforced concrete with a small amount of transverse reinforcement. The relation has the following simple form:
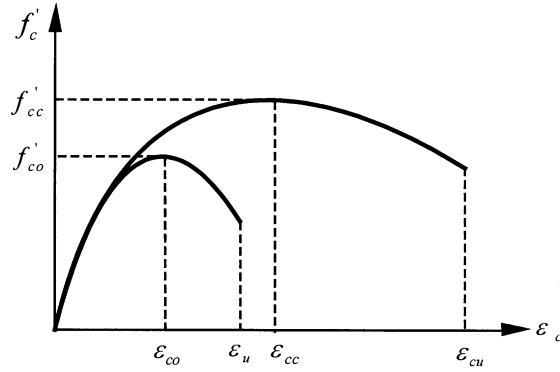
FIGURE 36.4 Idealized stress-strain curves for concrete in uniaxial compression.

$$
f_c = \begin{cases}
f'_{co}\left[\dfrac{2\varepsilon_c}{\varepsilon_{co}} - \left(\dfrac{\varepsilon_c}{\varepsilon_{co}}\right)^2\right] & \varepsilon_c \le \varepsilon_{co} \\[3mm]
f'_{co}\left[1 - \beta\left(\dfrac{\varepsilon_c - \varepsilon_o}{\varepsilon_u - \varepsilon_{co}}\right)\right] & \varepsilon_{co} < \varepsilon_c \le \varepsilon_u
\end{cases}
\tag{36.13}
$$

$$
\varepsilon_{co} = \frac{2f'_{co}}{E_c}
\tag{36.14}
$$

where f_c and ε_c are the concrete stress and strain; f'_{co} is the peak stress for unconfined concrete usually taken as the cylindrical compression strength f'_c; ε_{co} is strain at peak stress for unconfined concrete usually taken as 0.002; ε_u is the ultimate compression strain for unconfined concrete taken as 0.003; E_c is the modulus of elasticity of concrete; β is a reduction factor for the descending branch usually taken as 0.15. Note that the format of Eq. (36.13) can be also used for confined concrete if the concrete-confined peak stress f_{cc} and strain E_{cu} are known or assumed and substituted for f'_{co} and ε_u, respectively.

Confined Concrete — Mander's Model

Analytical models describing the stress–strain relationship for confined concrete depend on the confining transverse reinforcement type (such as hoops, spiral, or ties) and shape (such as circular, square, or rectangular). Some of those analytical models are more general than others in their applicability to various confinement types and shapes. A general stress–strain model (Figure 36.5) for confined concrete applicable (in theory) to a wide range of cross sections and confinements was proposed by Mander et al. [23,24] and has the following form:

$$
f_c = \frac{f'_{cc}(\varepsilon_c / \varepsilon_{cc}) r}{r - 1 + (\varepsilon_c / \varepsilon_{cc})^r}
\tag{36.15}
$$

$$
\varepsilon_{cc} = \varepsilon_{co}\left[1 + 5\left(\frac{f'_{cc}}{f'_{co}} - 1\right)\right]
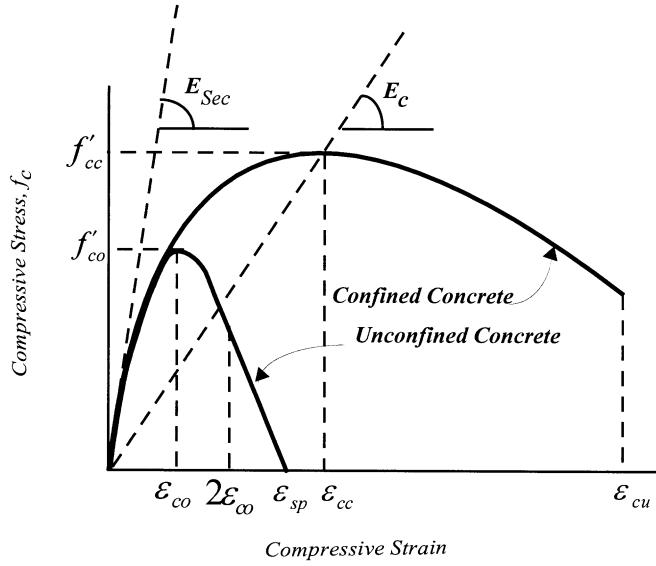\tag{36.16}
$$

FIGURE 36.5 Stress–strain curves — mander model.

$$r = \frac{E_c}{E_c - E_{\text{sec}}} \tag{36.17}$$

$$E_{\text{sec}} = \frac{f'_{cc}}{\varepsilon_{cc}} \tag{36.18}$$

where f'_{cc} and ε_{cc} are peak compressive stress and corresponding strain for confined concrete. f'_{cc} and ε_{cu} which depend on the confinement type and shape, are calculated as follows:

Confined Peak Stress

1. **For concrete circular section confined by circular hoops or spiral** (Figure 36.6a):

$$f'_{cc} = f'_{co}\left(2.254\sqrt{1 + \frac{7.94 f'_l}{f'_{co}}} - \frac{2 f'_l}{f'_{co}} - 1.254\right) \tag{36.19}$$

$$f'_l = \frac{1}{2} K_e \rho_s f_{yh} \tag{36.20}$$

$$K_e = \begin{cases} \left(1 - s'/2d_s\right)^2 / \left(1 - \rho_{cc}\right) & \text{for circular hoops} \\ \left(1 - s'/2d_s\right) / \left(1 - \rho_{cc}\right) & \text{for circular spirals} \end{cases} \tag{36.21}$$

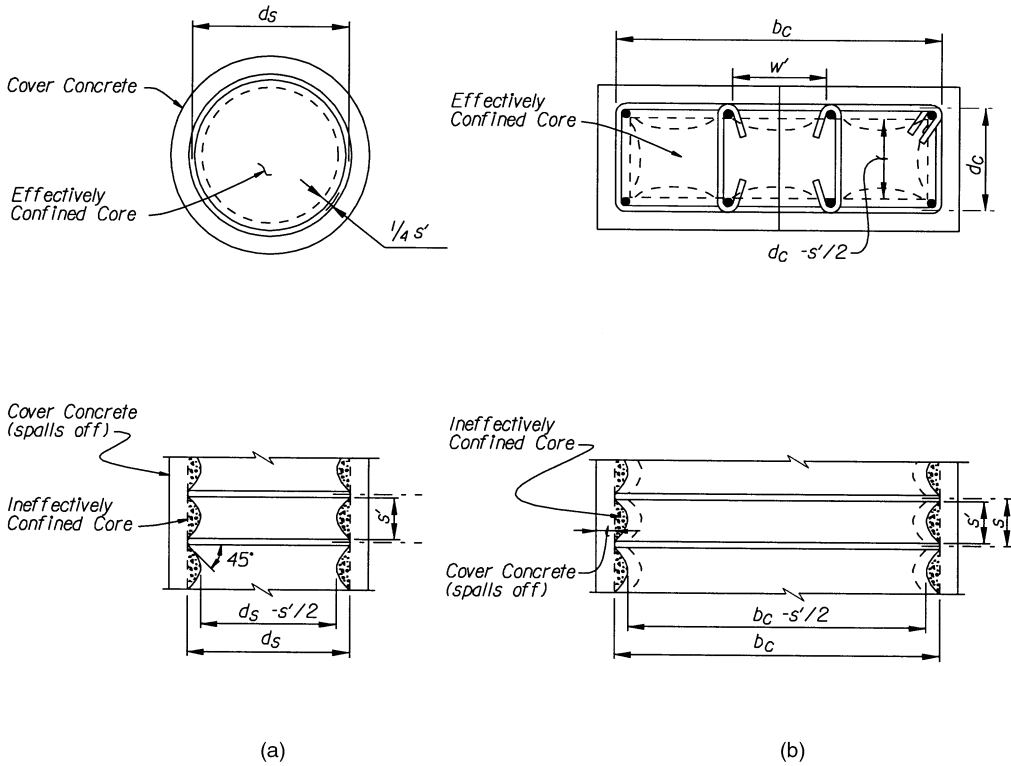$$\rho_s = \frac{4 A_{sp}}{d_s s} \tag{36.22}$$

FIGURE 36.6 Confined core for hoop reinforcement. (a) Circular hoop and (b) rectangular hoop reinforcement.

where f'_l is the effective lateral confining pressure; K_e is confinement effectiveness coefficient, f_{yh} is the yield stress of the transverse reinforcement, s' is the clear vertical spacing between hoops or spiral; s is the center-to-center spacing of the spiral or circular hoops; d_s is the centerline diameter of the spiral or hoops circle; ρ_{cc} is the ratio of the longitudinal reinforcement area to section core area; ρ_s is the ratio of the transverse confining steel volume to the confined concrete core volume; and A_{sp} is the bar area of transverse reinforcement.

2. **For rectangular concrete section confined by rectangular hoops** (Figure 36.6b)

The rectangular hoops may produce two unequal effective confining pressures f'_{lx} and f'_{ly} in the principal x and y direction defined as follows:

$$f'_{lx} = K_e\, \rho_x\, f_{yh} \tag{36.23}$$

$$f'_{ly} = K_e\, \rho_y\, f_{yh} \tag{36.24}$$

$$K_e = \frac{\left[1 - \sum_{i=1}^{n} \dfrac{(w'_i)^2}{6b_c d_c}\right]\left(1 - \dfrac{s'}{2b_c}\right)\left(1 - \dfrac{s'}{2d_c}\right)}{\left(1 - \rho_{cc}\right)} \tag{36.25}$$

$$\rho_x = \frac{A_{sx}}{s\, d_c} \tag{36.26}$$

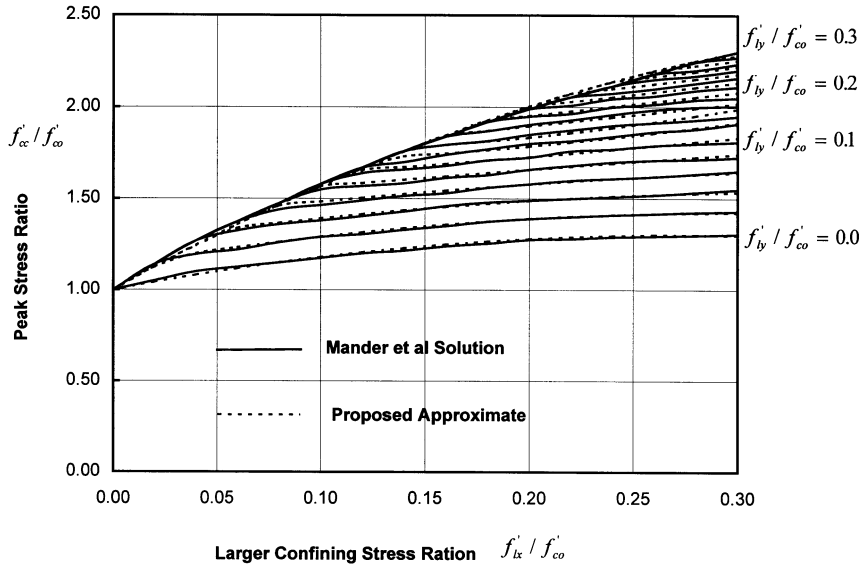$$\rho_y = \frac{A_{sy}}{s\, b_c} \tag{36.27}$$

FIGURE 36.7 Peak stress of confined concrete.

where f_{yh} is the yield strength of transverse reinforcement; w_i' is the ith clear distance between adjacent longitudinal bars; b_c and d_c are core dimensions to centerlines of hoop in x and y direction (where $b \geq d$), respectively; A_{sx} and A_{sy} are the total area of transverse bars in x and y direction, respectively.

Once f_{lx}' and f_{ly}' are determined, the confined concrete strength f_{cc}' can be found using the chart shown in Figure 36.7 with f_{lx}' being greater or equal to f_{ly}'. The chart depicts the general solution of the "five-parameter" multiaxial failure surface described by William and Warnke [26].

As an alternative to the chart, the authors derived the following equations for estimating f_{cc}':

$$f_{cc} = \begin{cases} A f_{lx}'^2 + B f_{lx}' + C & f_{ly}' < f_{lx}' \text{ and } f_{ly}' \leq 0.15 \\[2mm] \dfrac{f_{lx}' - f_{lx}'}{0.3 - f_{ly}'} D + C & f_{ly}' < f_{lx}' \text{ and } f_{ly}' > 0.15 \\[2mm] C & f_{ly}' = f_{lx}' \end{cases} \qquad (36.28)$$

$$A = 196.5 f_{lx}'^2 + 29.1 f_{lx}' - 4 \qquad (36.29)$$

$$B = -69.5 f_{lx}'^2 - 8.9 f_{lx}' + 2.2 \qquad (36.30)$$

$$C = -6.83 f_{lx}'^2 + 6.38 f_{lx}' + 1 \qquad (36.31)$$

$$D = -1.5 f_{lx}'^2 - 0.55 f_{lx}' + 0.3 \qquad (36.32)$$

Note that by setting $f_l' = 0.0$ in Eqs. (36.19), Eqs. (36.16) and (36.15) will produce to Mander's expression for unconfined concrete. In this case and for concrete strain $\varepsilon_c > 2\,\varepsilon_{co}$, a straight line which reaches zero stress at the spalling strain ε_{sp} is assumed.

Confined Concrete Ultimate Compressive Strain

Experiments have shown that a sudden drop in the confined concrete stress–strain curve takes place when the confining transverse steel first fractures. Defining the ultimate compressive strain as the longitudinal strain at which the first confining hoop fracture occurs, and using the energy balance approach, Mander et al. [27] produced an expression for predicting the ultimate compressive strain which can be solved numerically.

A conservative and simple equation for estimating the confined concrete ultimate strain is given by Priestley et al. [7]:

$$\varepsilon_{cu} = 0.004 + \frac{1.4\rho_s f_{yh}\varepsilon_{su}}{f'_{cc}} \tag{36.33}$$

where ε_{su} is the steel strain at maximum tensile stress. For rectangular section $\rho_s = \rho_x + \rho_y$ as defined previously. Typical values for ε_{cu} range from 0.012 to 0.05.

Equation (36.33) is formulated for confined sections subjected to axial compression. It is noted that when Eq. (36.33) is used for a section in bending or in combined bending and axial compression, then it tends to be conservative by a least 50%.

Chai et al. [28] used an energy balance approach to derive the following expression for calculating the concrete ultimate confined strain as

$$\varepsilon_{cu} = \varepsilon_{sp} + \begin{cases} \rho_s\varepsilon_{su}\dfrac{\gamma_2 J_{yh}}{\gamma_1 f'_{cc}} & \text{confined by reinconcement} \\[3mm] \rho_{sj}\varepsilon_{suj}\dfrac{\gamma_2 f_{yj}}{\gamma_1 f'_{cc}} & \text{confined by circular steel jackets} \end{cases} \tag{36.34}$$

where ε_{sp} is the spalling strain of the unconfined concrete (usually = 0.003 to 0.005), γ_1 is an integration coefficient of the area between the confined and unconfined stress–strain curves; and γ_2 is an integration coefficient of the area under the transverse steel stress–strain curve. The confining ratio for steel jackets $\rho_{sj} = 4t_j/(D_j - 2t_j)$; D_i and t_j are outside diameter and thickness of the jacket, respectively; f_{yj} is yield stress of the steel jacket. For high- and mild-strength steels and concrete compressive strengths of 4 to 6 ksi (27.58 to 41.37 MPa), Chai et al. [28] proposed the following expressions

$$\frac{\gamma_2}{\gamma_1} = \begin{cases} \dfrac{2000\rho_s}{\left(1+(1428\rho_s)^4\right)^{0.25}} & \text{for Grade 40 Steel} \\[4mm] \dfrac{2000\rho_s}{\left(1+(1480\rho_s)^{0.25}\right)^{0.4}} & \text{for Grade 60 Steel} \end{cases} \tag{36.35}$$

Confined Concrete — Hoshikuma's Model

In additional to Mander's model, Table 36.6 lists a stress–strain relationship for confined concrete proposed by Hoshikuma et al. [25]. The Hoshikuma model was based on the results of a series of experimental tests covering circular, square, and wall-type cross sections with various transverse reinforcement arrangement in bridge piers design practice in Japan.

36.4.1.2 Tension Stress-Strain Relationship

Two idealized stress–strain curves for concrete in tension is shown in Figure 36.8. For plain concrete, the curve is linear up to cracking stress f_r. For reinforced concrete, there is a descending branch

TABLE 36.6 Hoshikuma et al. [25] Stress–Strain Relationship of Confined Concrete

$$f_c = \begin{cases} E_c\varepsilon_c\left[1 - \dfrac{1}{n}\left(\dfrac{\varepsilon_c}{\varepsilon_{cc}}\right)^{n-1}\right] & \varepsilon_c \le \varepsilon_{cc} \\[2ex] f'_{cc} - E_{des}\left(\varepsilon_c - \varepsilon_{cc}\right) & \varepsilon_{cc} < \varepsilon_c \le \varepsilon_{cu} \end{cases}$$

$$n = \frac{E_c\varepsilon_{cc}}{E_c\varepsilon_{cc} - f'_{cc}} \; ; \; \varepsilon_{cu} = \varepsilon_{cc} + \frac{f'_{cc}}{2E_{des}} \; ; \; E_{des} = 11.2\frac{f'^2_{co}}{\rho_s f_{yh}}$$

$$\frac{f'_{cc}}{f'_{co}} = \begin{cases} 1.0 + 3.8\dfrac{\rho_s f_{yh}}{f'_{co}} & \text{for circular section} \\[2ex] 1.0 + 0.76\dfrac{\rho_s f_{yh}}{f'_{co}} & \text{for square section} \end{cases}$$

$$\varepsilon_{cc} = \begin{cases} 0.002 + 0.033\dfrac{\rho_s f_{sh}}{f'_{co}} & \text{for circular section} \\[2ex] 0.002 + 0.013\dfrac{\rho_s f_{sh}}{f'_{co}} & \text{for square section} \end{cases}$$
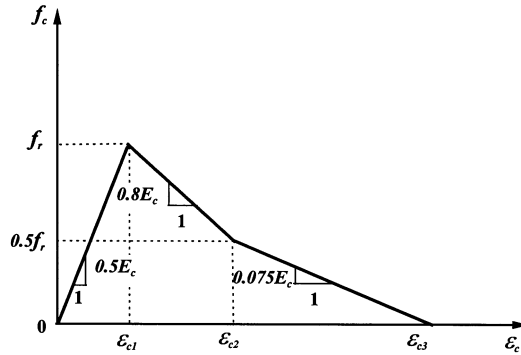

FIGURE 36.8   Idealized stress–strain curve of concrete in uniaxial tension.

because of bond characteristics of reinforcement. A trilinear expression proposed by Vebe et al. [29] is as follows:

$$f_c = \begin{cases} 0.5E_c\varepsilon_c & \varepsilon_c \ge \varepsilon_{c1} = 2f_r/E_c \\ f_r[1 - 0.8E_c(\varepsilon_c - 2f_r/E_c)] & \varepsilon_{c1} < \varepsilon_c \le \varepsilon_{c2} = 2.625f_r/E_c \\ f_r[0.5 - 0.075E_c(\varepsilon_c - 2.625f_r/4E_c)] & \varepsilon_c < \varepsilon_{c3} = 9.292f_r/E_c \end{cases} \qquad (36.36)$$

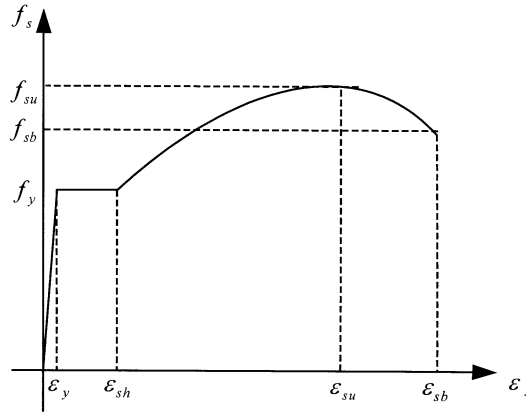where f_r is modulus of rupture of concrete.

FIGURE 36.9 Idealized stress–strain curve of structural steel and reinforcement.

36.4.2 Structural and Reinforcement Steel

For structural steel and nonprestressed steel reinforcement, its stress–strain relationship can be idealized as four parts: elastic, plastic, strain hardening, and softening, as shown in Figure 36.9. The relationship if commonly expressed as follows:

$$
f_s = \begin{cases}
E_s \varepsilon_s & 0 \le \varepsilon_s \le \varepsilon_y \\[2mm]
f_y & \varepsilon_{sy} < \varepsilon_s \le \varepsilon_{sh} \\[2mm]
f_y + \dfrac{\varepsilon_s - \varepsilon_{sh}}{\varepsilon_{su} - \varepsilon_{sh}}(f_{su} - f_y) & \varepsilon_{sh} < \varepsilon_s \le \varepsilon_{su} \\[2mm]
f_u \left[1 - \dfrac{\varepsilon_s - \varepsilon_{su}}{\varepsilon_{sb} - \varepsilon_{su}}(f_{su} - f_{sb}) \right] & \varepsilon_{cu} < \varepsilon_s \le \varepsilon_{sb}
\end{cases}
\tag{36.37}
$$

where f_s and ε_s is stress of strain in steel; E_s is the modulus of elasticity of steel; f_y and ε_y is yield stress and strain; ε_{sh} is hardening strain; f_{su} and ε_{su} is maximum stress and corresponding strain; f_{sb} and ε_{sb} are rupture stress and corresponding strain.

$$
\varepsilon_{sh} = \begin{cases}
14\,\varepsilon_y & \text{for Grade 40} \\[2mm]
5\,\varepsilon_y & \text{for Grade 60}
\end{cases}
\tag{36.38}
$$

$$
\varepsilon_{su} = \begin{cases}
0.14 + \varepsilon_{sh} & \text{for Grade 40} \\[2mm]
0.12 & \text{for Grade 60}
\end{cases}
\tag{36.39}
$$

For the reinforcing steel, the following nonlinear form can also be used for the strain-hardening portion [28]:

$$
f_s = f_y \left[\frac{m(\varepsilon_s - \varepsilon_{sh}) + 2}{60(\varepsilon_s - \varepsilon_{sh}) + 2} + \frac{(\varepsilon_s - \varepsilon_{sh})(60 - m)}{2(30r + 1)^2} \right] \quad \text{for } \varepsilon_{sh} < \varepsilon_s \le \varepsilon_{su}
\tag{36.40}
$$

$$m = \frac{(f_{su} / f_y)(30r+1)^2 - 60r - 1}{15r^2} \tag{36.41}$$

$$r = \varepsilon_{su} - \varepsilon_{sh} \tag{36.42}$$

$$f_{su} = 1.5 f_y \tag{36.43}$$

For both strain-hardening and -softening portions, Holzer et al. [30] proposed the following expression

$$f_s = f_y \left[1 + \frac{\varepsilon_s - \varepsilon_{sh}}{\varepsilon_{su} - \varepsilon_{sh}} \left(\frac{f_{su}}{f_y} - 1 \right) \exp \left(1 - \frac{\varepsilon_s - \varepsilon_{sh}}{\varepsilon_{su} - \varepsilon_{sh}} \right) \right] \qquad \text{for } \varepsilon_{sh} < \varepsilon_s \leq \varepsilon_{sb} \tag{36.44}$$

For prestressing steel, its stress–strain behavior is different from the nonprestressed steel. There is no obvious yield flow plateau in its response. The stress-stress expressions presented in Chapter 10 can be used in an analysis.

36.5 Nonlinear Section Analysis

36.5.1 Basic Assumptions and Formulations

The main purpose of section analysis is to study the moment–thrust–curvature behavior. In a nonlinear section analysis, the following assumptions are usually made:

- Plane sections before bending remain plane after bending;
- Shear and torsional deformation is negligible;
- Stress-strain relationships for concrete and steel are given;
- For reinforced concrete, a prefect bond between concrete and steel rebar exists.

The mathematical formulas used in the section analysis are (Figure 36.10):

Compatibility equations

$$\phi_x = \varepsilon / y \tag{36.45}$$

$$\phi_y = \varepsilon / x \tag{36.46}$$

Equilibrium equations

$$P = \int_A \sigma \, dA = \sum_{i=1}^{n} \sigma_i A_i \tag{36.47}$$

$$M_x = \int_A \sigma \, y \, dA = \sum_{i=1}^{n} \sigma_i y_i A_i \tag{36.48}$$

$$M_y = \int_A \sigma \, x \, dA = \sum_{i=1}^{n} \sigma_i x_i A_i \tag{36.49}$$
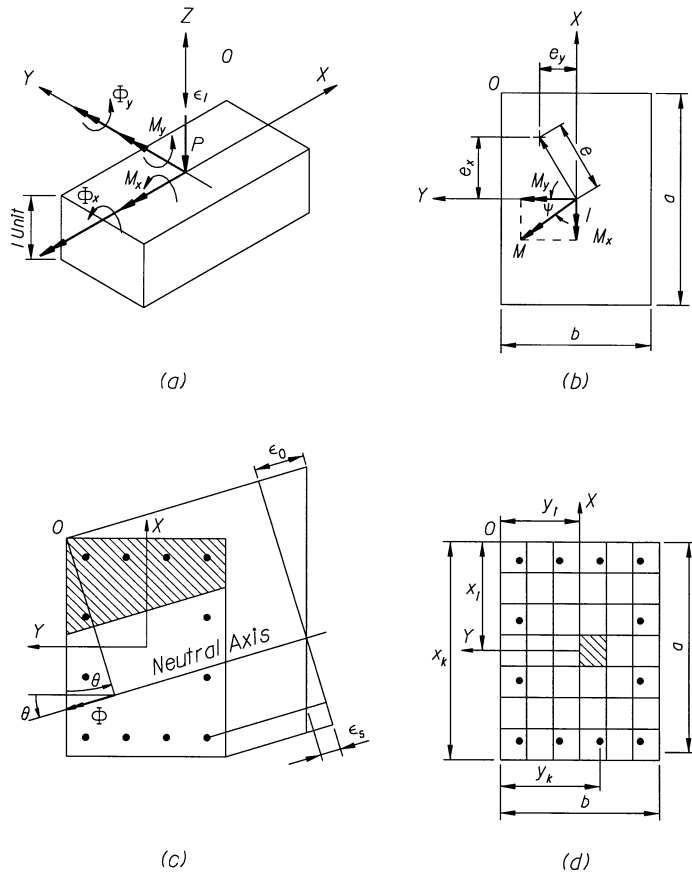
FIGURE 36.10 Moment–curvature–strain of cross section.

36.5.2 Modeling and Solution Procedures

For a reinforced-concrete member, the cross section is divided into a proper number of concrete and steel filaments representing the concrete and reinforcing steel as shown in Figure 36.10d. Each concrete and steel l filament is assigned its corresponding stress–strain relationships. Confined and unconfined stress–strain relationships are used for the core concrete and for the cover concrete, respectively.

For a structural steel member, the section is divided into steel filaments and a typical steel stress–strain relationship is used for tension and compact compression elements, and an equivalent stress–strain relationship with reduced yield stress and strain can be used for a noncompact compression element.

The analysis process starts by selecting a strain for the extreme concrete (or steel) fiber. By using this selected strain and assuming a section neutral axis (NA) location, a linear strain profile is constructed and the corresponding section stresses and forces are computed. Section force equilibrium is then checked for the given axial load. By changing the location of the NA, the process is repeated until equilibrium is satisfied. Once equilibrium is satisfied, for the assumed strain and the given axial load, the corresponding section moment and curvature are computed by Eqs. (36.48) and (36.49).

A moment–curvature (M–Φ) diagram for a given axial load is constructed by incrementing the extreme fiber strain and finding the corresponding moment and the associated curvature. An

interaction diagram (*M–P*) relating axial load and the ultimate moment is constructed by incrementing the axial load and finding the corresponding ultimate moment using the above procedure.

For a reinforced-concrete section, the yield moment is usually defined as the section moment at onset of yielding of the tension reinforcing steel. The ultimate moment is defined as the moment at peak moment capacity. The ultimate curvature is usually defined as the curvature when the extreme concrete fiber strain reaches ultimate strain or when the reinforcing rebar reaches its ultimate (rupture) strain (whichever takes place first). Figure 36.11a shows typical *M–P–Φ* curves for a reinforced-concrete section.

For a simple steel section, such as rectangular, circular-solid, and thin-walled circular section, a closed-form of *M–P–Φ* can be obtained using the elastic-perfectly plastic stress–strain relations [4, 31]. For all other commonly used steel section, numerical iteration techniques are used to obtain *M–P–Φ* curves. Figure 36.11b shows typical *M–P–Φ* curves for a wide-flange section.

36.5.3 Yield Surface Equations

The yield or failure surface concept has been conveniently used in inelastic analysis to describe the full plastification of steel and concrete sections under the action of axial force combined with biaxial bending. This section will present several yield surface expressions for steel and concrete sections suitable for use in a nonlinear analysis.

36.5.3.1 Yield Surface Equations for Concrete Sections

The general interaction failure surface for a reinforced-concrete section with biaxial bending, as shown in Figure 36.12a can be approximated by a nondimensional interaction equation [32]:

$$\left(\frac{M_x}{M_{xo}} \right)^m + \left(\frac{M_y}{M_{yo}} \right)^n = 1.0 \tag{36.50}$$

where M_x and M_y are bending moments about x–x and y–y principal axes, respectively; M_{xo} and M_{yo} are the uniaxial bending capacity about the x–x and y–y axes under axial load P; the exponents m and n depend on the reinforced-concrete section properties and axial force. They can be determined by a numerical analysis or experiments. In general, the values of m and n usually range from 1.1 to 1.4 for low and moderate axial compression.

#### 36.5.3.2 Yield Surface Equation for Doubly Symmetrical Steel Sections

The general shape of yield surface for a doubly symmetrical steel section as shown in Figure 36.12b can be described approximately by the following general equation [33]

$$\left(\frac{M_x}{M_{pcx}} \right)^{\alpha_x} + \left(\frac{M_y}{M_{pcy}} \right)^{\alpha_y} = 1.0 \tag{36.51}$$
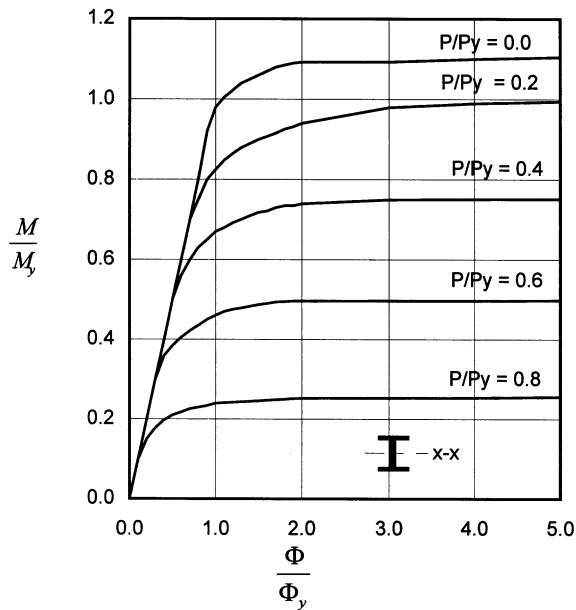
where M_{pcx} and M_{pcy} are the moment capacities about respective axes, reduced for the presence of axial load; they can be obtained by the following formulas:

$$M_{pcx} = M_{px} \left[1 - \left(\frac{P}{P_y} \right)^{\beta_x} \right] \tag{36.52}$$

$$M_{pcy} = M_{py} \left[1 - \left(\frac{P}{P_y} \right)^{\beta_y} \right] \tag{36.53}$$
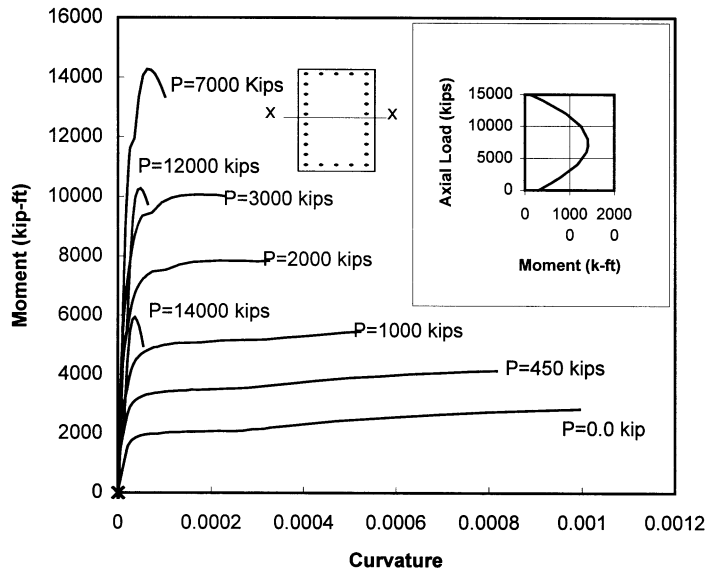
FIGURE 36.11 Moment–thrust–curvature curve. (a) Reinforced concrete section (b) steel I-section.

where P is the axial load; M_{px} and M_{py} are the plastic moments about x–x and y–y principal axes, respectively; α_x, α_y, β_x, and β_y are parameters that depend on cross-sectional shapes and area distribution and are listed in Table 36.7.

Equation (36.51) represents a smooth and convex surface in the three-dimensional stress-result-ant space. It is easy to implement in a computer-based structural analysis.
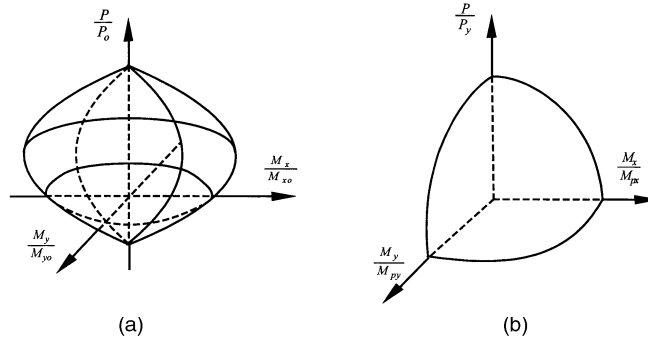
FIGURE 36.12 General yield surfaces. (a) Reinforced concrete section; (b) steel section.

TABLE 36.7 Parameters for Doubly Symmetrical Steel Sections

Section Types	α_x	α_y	β_x	β_y
Solid rectangular	$1.7 + 1.3\ (P/P_y)$	$1.7 + 1.3\ (P/P_y)$	2.0	2.0
Solid circular	2.0	2.0	2.1	2.1
I-shape	2.0	$1.2 + 2\ (P/P_y)$	1.3	$2 + 1.2\ (A_w/A_f)$
Thin-walled box	$1.7 + 1.5\ (P/P_y)$	$1.7 + 1.5\ (P/P_y)$	$2 - 0.5\ \overline{B} \geq 1.3$	$2 - 0.5\ \overline{B} \geq 1.3$
Thin-walled circular	2.0	2.0	1.75	1.75

Where $\overline{B}$ is the ratio of width to depth of the box section with respect to the bending axis.

Orbison [15] developed the following equation for a wide-flange section by trial and error and curve fitting:

$$
1.15\left(\frac{P}{P_y}\right)^2 + \left(\frac{M_x}{M_{px}}\right)^2 + \left(\frac{M_y}{M_{py}}\right)^4 + 3.67\left(\frac{P}{P_y}\right)\left(\frac{M_x}{M_{px}}\right)^2
$$

$$
+ 3.0\left(\frac{P}{P_y}\right)^2\left(\frac{M_y}{M_{py}}\right)^2 + 4.65\left(\frac{M_x}{M_{px}}\right)^4\left(\frac{M_y}{M_{py}}\right)^2 = 1.0
$$

(36.54)

36.6 Nonlinear Frame Analysis

Both the first-order and second-order inelastic frame analyses can be categorized into three types of analysis: (1) elastic–plastic hinge, (2) refined plastic hinge, and (3) distributed plasticity. This section will discuss the basic assumptions and applications of those analyses.

36.6.1 Elastic–Plastic Hinge Analysis

In an elastic-plastic hinge (lumped plasticity) analysis, material inelasticity is taken into account using concentrated "zero-length" plastic hinges. The traditional plastic hinge is defined as a zero-length point along the structure member which can maintain plastic moment capacity and rotate freely. When the section reaches its plastic capacity (for example, the yield surface as shown in Figures 36.12 or 36.13), a plastic hinge is formed and the element stiffness is adjusted [34, 35] to reflect the hinge formation. For regions in a framed member away from the plastic hinge, elastic behavior is assumed.
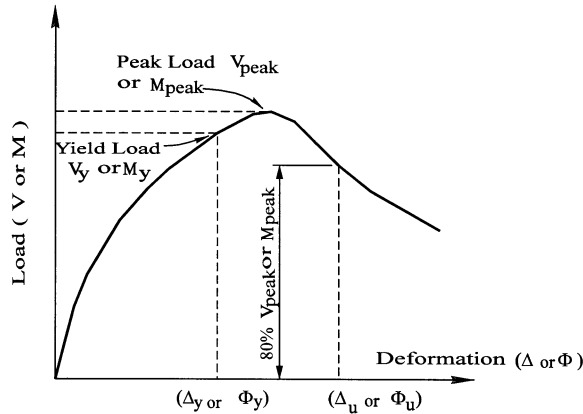
Peak Load V_{peak}
or M_{peak}

Yield Load
V_y or M_y

Load (V or M)

80% V_{peak} or M_{peak}

Deformation (Δ or Φ)

$(\Delta_{y \text{ or }} \Phi_y)$ $(\Delta_u \text{ or } \Phi_u)$

FIGURE 36.13   Load-deformation curves.

For a framed member subjected to end forces only, the elastic–plastic hinge method usually requires only one element per member making the method computationally efficient. It does not, however, accurately represent the distributed plasticity and associated $P\text{-}\delta$ effects. This analysis predicts an upper-bound solution (see Figure 36.1).

36.6.2   Refined Plastic Hinge Analysis

In the refined plastic hinge analysis [36], a two-surface yield model considers the reduction of plastic moment capacity at the plastic hinge (due to the presence of axial force) and an effective tangent modulus accounts for the stiffness degradation (due to distributed plasticity along a frame member). This analysis is similar to the elastic–plastic hinge analysis in efficiency and simplicity and, to some extent, also accounts for distributed plasticity. The approach has been developed for advanced design of steel frames, but detailed considerations for concrete structures still need to be developed.

36.6.3   Distributed Plasticity Analysis

Distributed plasticity analysis models the spread of inelasticity through the cross sections and along the length of the members. This is also referred to as plastic zone analysis, spread-of-plasticity analysis, and elastoplastic analysis by various researchers. In this analysis, a member needs to be subdivided into several elements along its length to model the inelastic behavior more accurately. There are two main approaches which have been successfully used to model plastification of members in a second-order distributed plasticity analysis:

1. Cross-sectional behavior is described as an input for the analysis by means of moment–thrust–curvature (M–P–Φ) and moment–trust–axial strain (M–P–ε) relations which may be obtained separately from section analysis as discussed in Section 36.5 or approximated by closed-form expressions [31].
2. Cross sections are subdivided into elemental areas and the state of stresses and strains are traced explicitly using the proper stress–strain relations for all elements during the analysis.

In summary, the elastic–plastic hinge analysis is the simplest one, but provides an upper-bound solution. Distributed plasticity analysis is considered the most accurate and is generally computationally intensive for larger and complex structures. Refined plastic hinge analysis seems to be an alternative that can reasonably achieve both computational efficiency and accuracy.

36.7 Practical Applications

In this section, the concept and procedures of displacement-based design and the bases of the static push-over analysis are discussed briefly. Two real bridges are analyzed as examples to illustrate practical application of the nonlinear static push-over analysis approach for bridge seismic design. Additional examples and detailed discussions of nonlinear bridge analysis can be found in the literature [7, 37].

36.7.1 Displacement-Based Seismic Design

36.7.1.1 Basic Concept

In recent years, displacement-based design has been used in the bridge seismic design practice as a viable alternative approach to strength-based design. Using displacements rather than forces as a measurement of earthquake damage allows a structure to fulfill the required function (damage-control limit state) under specified earthquake loads.

In a common design procedure, one starts by proportioning the structure for strength and stiffness, performs the appropriate analysis, and then checks the displacement ductility demand against available capacity. This procedure has been widely used in bridge seismic design in California since 1994. Alternatively, one could start with the selection of a target displacement, perform the analysis, and then determine strength and stiffness to achieve the design level displacement. Strength and stiffness do not enter this process as variables; they are the end results [38, 39].

In displacement-based design, the designer needs to define a criterion clearly for acceptable structural deformation (damage) based on postearthquake performance requirements and the available deformation capacity. Such criteria are based on many factors including structural type and importance.

36.7.1.2 Available Ultimate Deformation Capacity

Because structural survival without collapse is commonly adopted as a seismic design criterion for ordinary bridges, inelastic structural response and some degradation in strength can be expected under seismic loads. Figure 36.13 shows a typical load–deformation curve. A gradual degrading response as shown in Figure 36.13 can be due to factors such as P-Δ effects and/or plastic hinge formulation. The available ultimate deformation capacity should be based on how great a reduction (degradation) in structure load-carrying capacity response can be tolerated [21].

In general, the available ultimate deformation capacity can be referred to as the deformation that a structure can undergo without losing significant load-carrying capacity [40]. It is, therefore, reasonable to define available ultimate deformation as that deformation when the load-carrying capacity has been reduced by an acceptable amount after the peak load, say, 20%, as shown in Figure 36.13. This acceptable reduction amount may vary depending on required performance criteria of the particular case.

The available deformation capacity based on the design criteria requirements needs not correspond to the ultimate member or system deformation capacity. For a particular member cross section, the ultimate deformation in terms of the curvature depends on the shape, material properties, and loading conditions of the section (i.e., axial load, biaxial bending) and corresponds to the condition when the section extreme fiber reaches its ultimate strain (ε_{cu} for concrete and ε_{sp} for steel). The available ultimate curvature capacity ϕ_u can be chosen as the curvature that corresponds to the condition when section moment capacity response reduces by, say, 20%, from the peak moment.

For a framed structure system, the ultimate deformation in terms of the lateral displacement depends on structural configurations, section behavior, and loading conditions and corresponds to a failure state of the frame system when a collapse mechanism forms. The available lateral displacement capacity Δ_u

can be chosen as the displacement that corresponds to the condition when lateral load-carrying capacity reduces by some amount, say, 20%, from its peak load. In current seismic design practice in California, the available frame lateral displacement capacity commonly corresponds to the first plastic hinge reaching its ultimate rotational capacity.

36.7.1.3 Analysis Procedures

Seismic analysis procedures used in displacement-based design can be divided into three groups:

Group I: Seismic displacement and force demands are estimated from an elastic dynamic time history or a response spectrum analysis with effective section properties. For concrete structures, cracked section properties are usually used to determine displacement bent demands, and gross section properties are used to determine force demands. Strength capacity is evaluated from nonlinear section analysis or other code-specified methods, and displacement capacity is obtained from a static nonlinear push-over analysis.

Group II: Seismic displacement demand is obtained from a specified response spectrum and initial effective stiffness or a substitute structural model [38] considering both the effective stiffness and the effective damping. Effective stiffness and displacement capacity are estimated from a nonlinear static push-over analysis.

Group III: A nonlinear inelastic dynamic time history analysis is performed. Bridge assessment is based on displacement (damage) comparisons between analysis results and the given acceptance criteria. This group of analyses is complex and time-consuming and used only for important structures.

36.7.2 Static Push-Over Analysis

In lieu of a nonlinear time history dynamic analysis, bridge engineers in recent years have used static push-over analyses as an effective and simple alternative when assessing the performance of existing or new bridge structures under seismic loads. Given the proper conditions, this approximate alternative can be as reliable as the more accurate and complex ones. The primary goal of such an analysis is to determine the displacement or ductility capacity which is then compared with displacement or ductility demand obtained for most cases from linear dynamic analysis with effective section properties. However, under certain conditions, the analysis can also be used in the assessment of the displacement demand, as will be illustrated in the examples to follow.

In this analysis, a stand-alone portion from a bridge structure (such as bent-frame with single or multicolumns) is isolated and statically analyzed taking into account whatever nonlinear behavior deemed necessary (most importantly and commonly, material and geometric nonlinear behavior). The analysis can utilize any of the modeling methods discussed in Section 36.6, but plastic hinges or distributed plasticity models are commonly used. The analytical frame model is first subjected to the applied tributary gravity load and then is pushed laterally in several load (or displacement) increments until a collapse mechanism or a given failure criterion is reached. Figure 36.14 shows a flowchart outlining a procedure using static push-over analysis in seismic design and retrofit evaluation.

When applying static push-over analysis in seismic design, it is assumed that such analysis can predict with reasonable accuracy the dynamic lateral load–displacement behavior envelope, and that an elastic acceleration response spectrum can provide the best means for establishing required structural performance.

36.7.3 Example 36.1 — Reinforced Concrete Multicolumn Bent Frame with P-Δ Effects

Problem Statement

The as-built details of a reinforced concrete bridge bent frame consisting of a bent cap beam and two circular columns supported on pile foundations are shown in Figure 36.15. An as-built unconfined
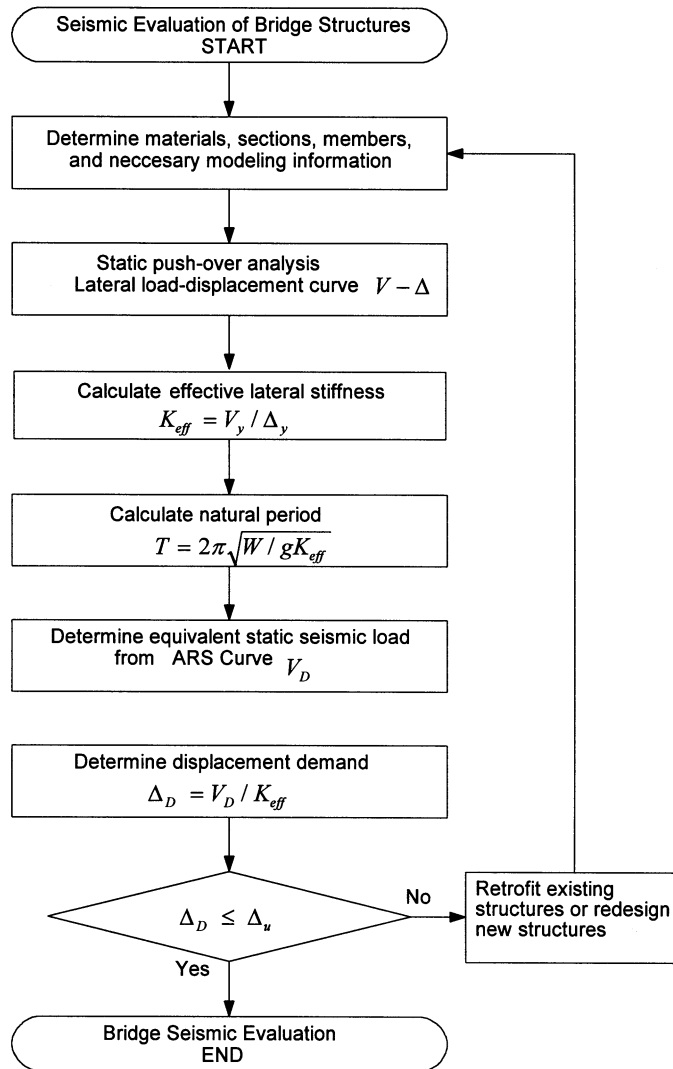
FIGURE 36.14 An alternative procedure for bridge seismic evaluation.

concrete strength of 5 ksi (34.5 MPa) and steel strength of 40 ksi (275.8 MPa) are assumed. Due to lack of adequate column transverse reinforcement, the columns are retrofitted with 0.5-in. (12.7-mm)-thick steel jacket. The bottom of the column is assumed to be fixed, however, since the footing lacks top mat and shear reinforcement, the bottom with a pinned connection is also to be considered. The frame is supported on a stiff pile–foundation and the soil–foundation–structure interaction is to be ignored.

Use static nonlinear push-over analysis to study the extent of the $P\text{-}\Delta$ effect on the lateral response of the bent frame when the columns are assumed fixed at the base in one case and pinned in another case. Assume the columns are retrofitted with steel jacket in both cases and determine if the footing retrofit is also required. Use 0.7 g ground acceleration and the ARS spectrum with 5% damping shown in Figure 36.16.

Analysis Procedure

The idealized bent frame, consisting of the cap beam and the two retrofitted column members, is discretized into a finite number of beam elements connected at joints, as shown in Figure 36.17.
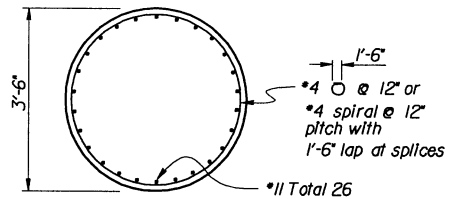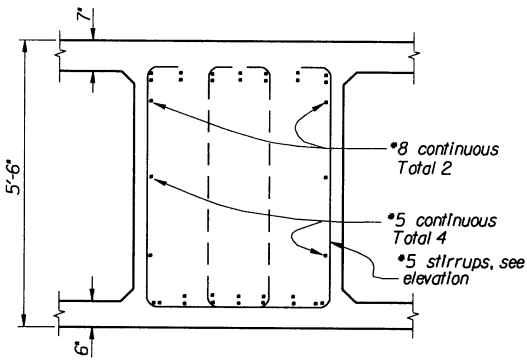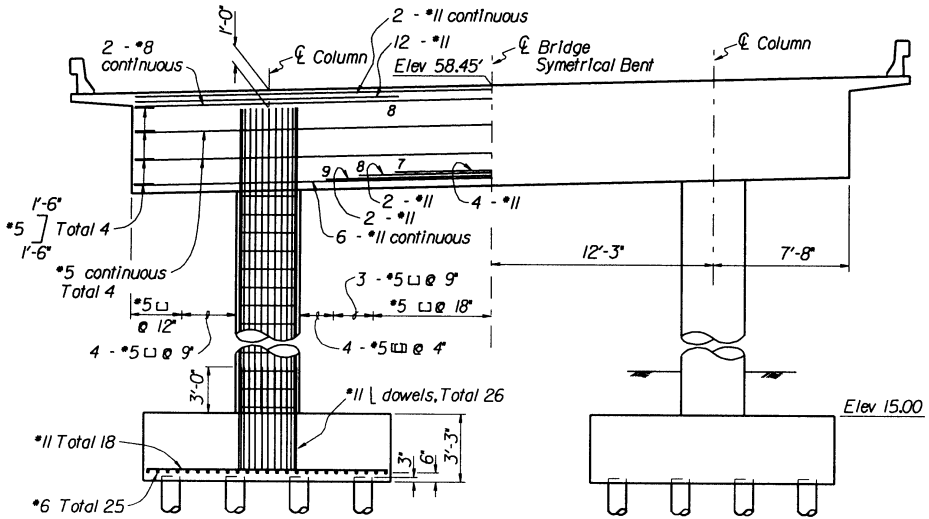
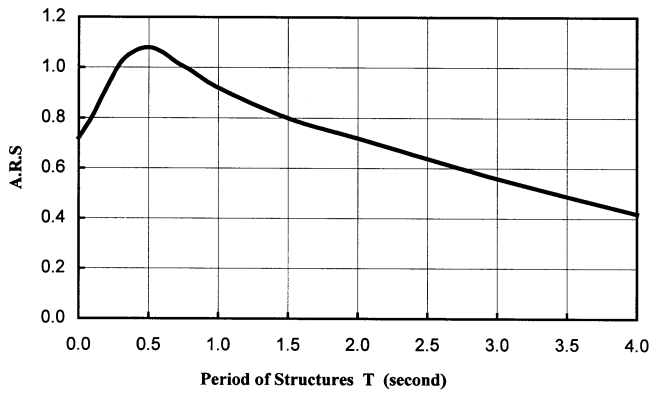**FIGURE 36.15** As-built plan — Example 36.1.

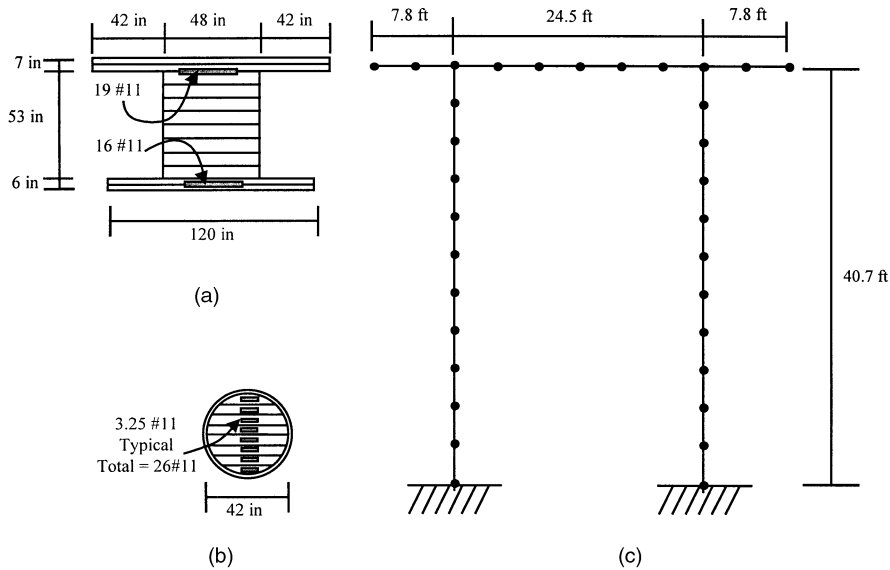**FIGURE 36.16** Specific ars curve — Example 36.1.

FIGURE 36.17 Analytical model — Example 36.1. (a) Local layered cab beam section: 12 concrete and 2 steel layers; (b) layered column section: 8 concrete and 8 steel layers; (c) discretized frame model.

The idealized column and cap beam cross sections are divided into several concrete layers and reinforcing steel layers as shown. Two different concrete material properties are used for the column and cap beam cross sections. The column concrete properties incorporated the increase in concrete ultimate stress and strain due to the confinement provided by the steel jacket. In this study the column confined ultimate concrete compressive stress and strain of 7.5 ksi (51.7 MPa) and 0.085 are used respectively. The total tributary superstructure dead load of 1160 kips (5160 kN) is applied uniformly along the length of the cap beam. The frame is pushed laterally in several load increments until failure is reached.

For this study, failure is defined as the limit state when one of the following conditions first take place:

1. A concrete layer strain reaches the ultimate compressive strain at any member section;
2. A steel layer strain reaches the rupture strain at any member section;
3. A 20% reduction from peak lateral load of the lateral load response curve (this condition is particularly useful when considering P-Δ).

The lateral displacement corresponding to this limit state at the top of the column defines the frame failure (available) displacement capacity.

A nonlinear analysis computer program NTFrame [41, 42] is used for the push-over analysis. The program is based on distributed plasticity model and the P-Δ effect is incorporated in the model second-order member stiffness formulation.

Discussion of the Results

The resulting frame lateral load vs. displacement responses are shown in Figures 36.18 for the cases when the bottom of the column is fixed and pinned. Both cases will be discussed next, followed by concluding remarks.

Column Fixed at Bottom Case
In this case the column base is modeled with a fixed connection. The lateral response with and without the P-Δ effect is shown in Figure 36.18a. The sharp drop in the response curve is due to several extreme concrete layers reaching their ultimate compressive strain at the top of the column.
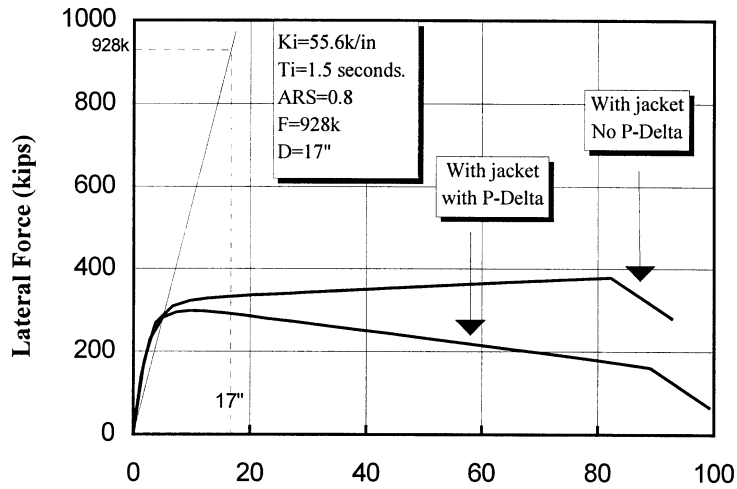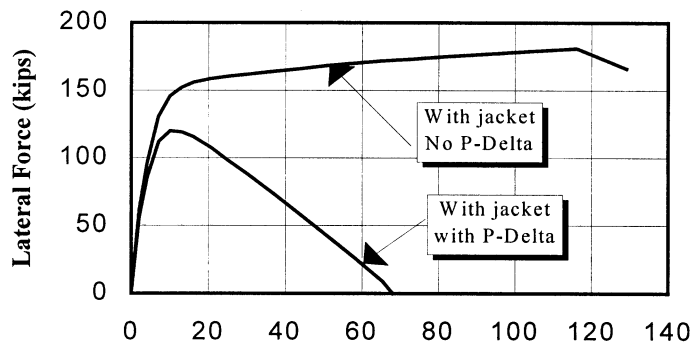
FIGURE 36.18 Lateral load vs. displacement responses — Example 36.1. Lateral response (a) fixed column (b) with penned column.

The effect of P-Δ at failure can be seen to be considerable but not as severe as shown in Figure 36.18b with the pinned connection. Comparing Figures 36.19a and b, one can observe that fixing the bottom of the column resulted in stiffer structural response.

Using the curve shown in Figure 36.18a, the displacement demand for the fixed column case with P-Δ effect is calculated as follows:

Step 1: Calculate the Initial Effective Stiffness K_{eff}

The computer results showed that the first column extreme longitudinal rebar reached yield at lateral force of 928 kips (4128 kN) at a corresponding lateral yield displacement of 17 in. (431.8 mm), therefore

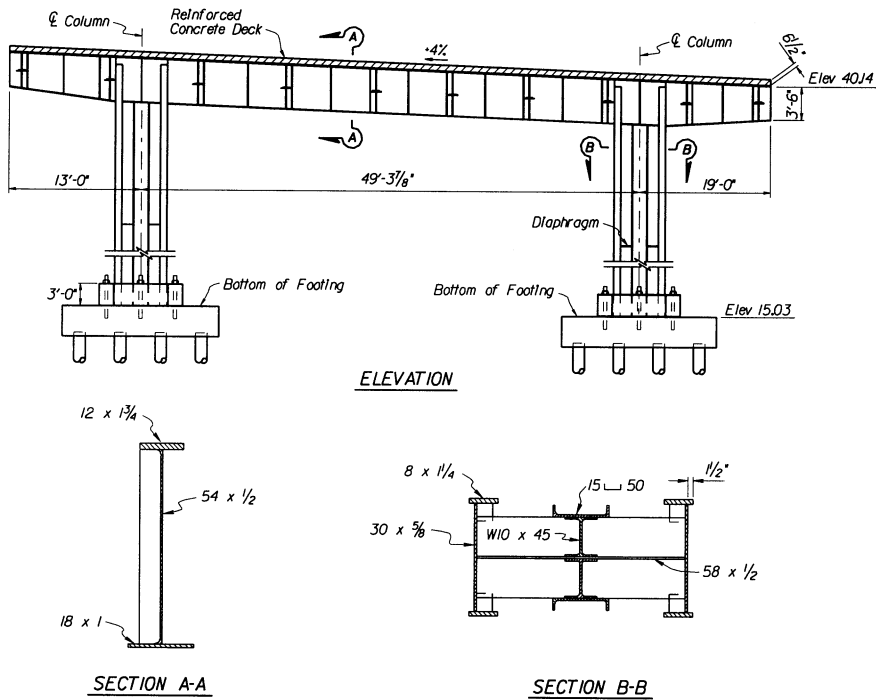$$K_{\text{eff}} = 928/17 = 55 \text{ kips/in. (9.63 kN/mm)}$$

FIGURE 36.19 As-built plane — Example 36.2.

Step 2: Calculate an Approximate Fundamental Period T_f

$$T_f = 0.32 \sqrt{\frac{W}{K_{\text{eff}}}} = 0.32 \sqrt{\frac{1160}{55}} = 1.5 \text{ s}$$

Step 3: Determine the Damped Elastic Acceleration Response Spectrum (ARS) at the Site in *g*'s

By using the given site spectrum shown in and the above calculated period, the corresponding ARS for 5% damping is 0.8.

Step 4: Calculate the Displacement Demand D_d

$$D_d = \frac{ARS(W)}{K_{eff}} = \frac{0.8(1160)}{55} = 16.9 \text{ in. (429.3 m)}$$

(in this case the yield and demand displacements are found to be practically equal).

In much of the seismic design practice in California, the effect of $P\text{-}\Delta$ is usually ignored if the $P\text{-}\Delta$ moment is less than 20% of the design maximum moment capacity. Adopting this practice and assuming the reduction in the moment is directly proportional to the reduction in the lateral force, one may conclude that at displacement demand of 16.9 in. (429.3 mm), the reduction in strength (lateral force) is less then 20%, and as a result the effects of $P\text{-}\Delta$ are negligible.

The displacement demand of 16.9 in. (429.3 mm) is less than the failure state displacement capacity of about 40 in. (1016 mm) (based on a 20% lateral load reduction from the peak). Note that for the fixed bottom case with $P\text{-}\Delta$, the displacement when the extreme concrete layer at the top of the column reached its ultimate compressive strain is about 90 in. (2286 mm).

Column Pinned at Bottom Case

In this case the column bottom is modeled with a pinned connection. Note that the pinned condition assumption is based on the belief that in the event of a maximum credible earthquake the column/footing connection would quickly degenerate (degrade) and behave like a pinned connection. The resulting lateral responses with and without the P-Δ effect are shown in Figure 36.18b. In this case the effects of P-Δ is shown to be quite substantial.

When considering the response without the P-Δ one obtains a displacement demand of 38 in. (965.2 mm) (based on a calculated initial stiffness of 18.5 kips/in. (3.24 kN/mm) and a corresponding structure period of 2.5 s). This displacement demand is well below the ultimate (at failure) displacement capacity of about 115 in. (2921 mm). As a result, one would conclude that the retrofit measure of placing a steel jacket around the column with no footing retrofit is adequate.

The actual response, however, is the one that includes the P-Δ effect. In this case the effect of P-Δ resulted in a slight change in initial stiffness and frame period — 15.8 kips/in. (2.77 kN/mm) and 2.7 s, respectively. However, beyond the initial stages, the effects are quite severe on the load–displacement response. The failure mode in this case will most likely be controlled by dynamic instability of the frame. MacRae et al. [43] performed analytical studies of the effect of P-Δ on single-degree-of-freedom bilinear oscillators (i.e., single-column frame) and proposed some procedures to obtain a limiting value at which the structure becomes dynamically unstable. The process requires the generation of the proper hysteresis loops and the determination of what is termed the *effective bilinear stiffness factor.* Setting aside the frame dynamic instability issue, the calculated initial stiffness displacement demand is about 38 in. (965.2 mm) and the displacement capacity at 20% reduction from peak load is 24 in. (609.6 mm).

Referring to the curves with P-Δ in Figure 36.18, it is of interest to mention, as pointed out by Mahin and Boroschek [44], that continued pushing of the frame will eventually lead to a stage when the frame structure becomes statically unstable. At that stage the forces induced by the P-Δ effect overcome the mechanical resistance of the structure. Note that the point when the curve with P-Δ effect intersects the displacement-axis in (as shown Figure 36.19b) will determine the lateral displacement at which the structure becomes statically unstable. Dynamic instability limits can be 20 to 70% less than the static instability depending on the ground motion and structural characteristic [44]. Note that dynamic instability is assumed not to be a controlling factor in the previous case with fixed column.

In conclusion, if the as-built column–footing connection can support the expected column moment obtained from the fixed condition case (which is unlikely), then retrofitting the column with steel jacket without footing retrofit is adequate. Otherwise, the footing should also be retrofitted to reduce (limit) the effect of P-Δ.

It should be pointed out that in this example the analysis is terminated at the completion of the first plastic hinge (conservative), whereas in other types of push-over analysis such as event-to-event analysis, the engineer may chose to push the frame farther until it forms a collapse mechanism. Also, unlike the substitute structure procedure described by Priestly et al. [7] in which both the effective system stiffness and damping ratio are adjusted (iterated) several times before final displacement demand is calculated, here only the initial effective stiffness and a constant specified structure damping are used.

As a final remark, the P-Δ effect in bridge analysis is normally assumed small and is usually ignored. This assumption is justified in most cases under normal loading conditions. However, as this example illustrated, under seismic loading, the P-Δ effect should be incorporated in the analysis, when large lateral displacements are expected before the structure reaches its assumed failure state. In the design of a new bridge, the lateral displacement and the effect of P-Δ can be controlled. When assessing an existing bridge for possible seismic retrofit, accurate prediction of the lateral displacement with P-Δ effects can be an essential factor in determining the retrofit measures required.
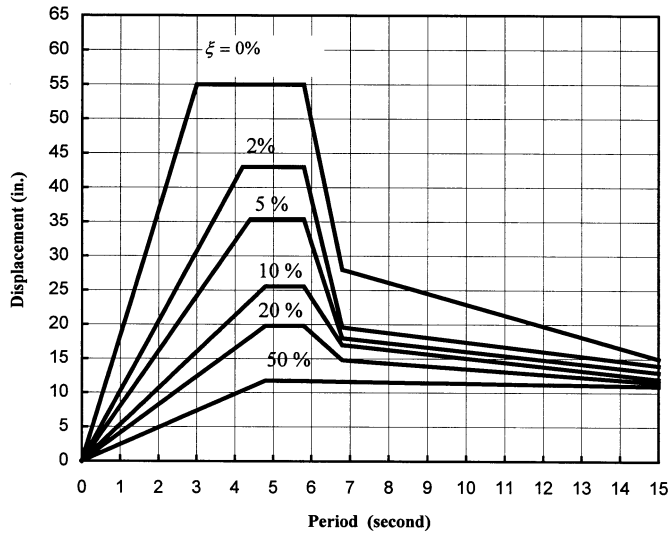
FIGURE 36.20 Displacement Response spectra — Example 36.2.

36.7.4 Example 36.2 — Steel Multicolumn Bent Frame Seismic Evaluation

Problem Statement

The as-built details of a steel bridge bent frame consisting of a bent cap plate girder and two builtup columns supported on a stiff pile–foundation, as shown in Figure 36.19. Steel is Grade 36. Site-specific displacement response spectra are given in Figure 36.20. For simplicity and illustration purposes, fixed bases of columns are assumed and the soil–foundation–structure interaction is ignored.

Evaluate lateral displacement capacity by using static nonlinear push-over analysis. Estimate seismic lateral displacement demands by using the substitute structure approach considering both the effective stiffness and the effective damping. The effective damping ξ can be calculated by Takeda's formula [45]:

$$\xi = 0.05 + \frac{\left(1 - \dfrac{0.95}{\sqrt{\mu_{\Delta d}}} - 0.05\sqrt{\mu_{\Delta d}}\right)}{\pi} \tag{36.55}$$

$$\mu_{\Delta d} = \frac{\Delta_{ud}}{\Delta_y} \tag{36.56}$$

where $\mu_{\Delta d}$ is displacement ductility demand; Δ_{ud} and Δ_y are displacement demand and yield displacement, respectively.

Analysis Modeling

The bent frame members are divided into several beam elements as shown in Figure 36.21. The properties of beam elements are defined by two sets of relationships for moment–curvature, axial force–strain, and torsion–twist for the cap beam and columns, respectively. The available ultimate curvature is assumed as 20 times yield curvature. The total tributary superstructure dead load of 800 kips (3558 kN) is applied at longitudinal girder locations. A lateral displacement is applied incrementally at the top of the bent column until a collapse mechanism of the bent frame is formed.
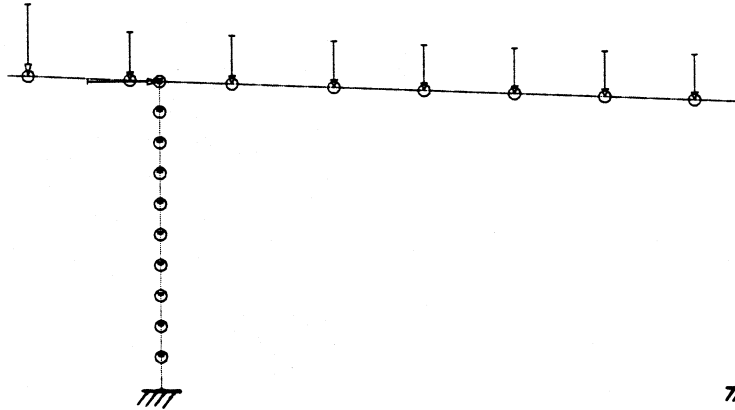
FIGURE 36.21   Analytical model — Example 36.2.

Displacement Capacity Evaluation

The displacement capacity evaluation is performed by push-over analysis using the ADINA [46] analysis program. Large displacements are considered in the analysis. The resulting lateral load vs. displacement response at the top of columns is shown in Figures 36.22. The sudden drops in the response curve are due to the several beam elements reaching their available ultimate curvatures. The yield displacement $\Delta_y = 1.25$ in. (31.8 mm) and the available ultimate displacement capacity (corresponding to a 20% reduction from the peak lateral load) $\Delta_u = 2.61$ in. (66.3 mm) are obtained.

Displacement Demand Estimation

A substitute structure approach with the effective stiffness and effective damping will be used to evaluate displacement demand.

1. Try $\Delta_{ud} = 3$ in. (76.2 mm); from Figure 36.20, Eqs. (36.55) and (36.56), we obtain

$$k_{\text{eff}} \quad 3 \quad 200 \text{ kips/in. (35.04 kN/mm)}$$

$$T_{\text{eff}} = 0.32 \sqrt{\frac{W(\text{kips})}{k_{\text{eff}}(\text{kips/in.})}} = 0.32 \sqrt{\frac{800}{200}} = 0.64 \text{ (s)}$$

$$\mu_{\Delta d} = \frac{\Delta_{ud}}{\Delta_y} = \frac{3}{1.25} = 2.4$$

$$\xi = 0.05 + \frac{\left(1 - \dfrac{0.95}{\sqrt{2.4}} - 0.05\sqrt{2.4}\right)}{\pi} = 0.15$$

   From Figure 36.20, find $\Delta_d = 2.5$ in. $< \Delta_{ud} = 3$ in. (76.2 mm).

2. Try $\Delta_{ud} = 2.5$ in. (63.5 mm); from Figures 36.20 and 36.22 Eqs. (36.55), and (36.56), we obtain
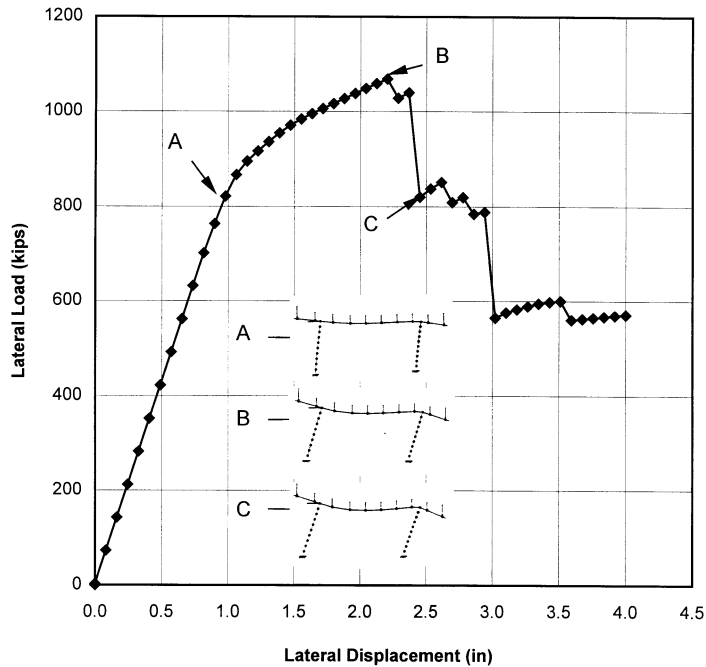
FIGURE 36.22 Lateral load vs. displacement — Example 36.2.

$$K_{\text{eff}} \quad 2.5 \qquad 332 \text{ kips/in. (58.1 kN/mm)}$$

$$T_{\text{eff}} = 0.32 \sqrt{\frac{W(\text{kips})}{K_{eff}(\text{kips/in.})}} = 0.32 \sqrt{\frac{800}{332}} = 0.50$$

$$\mu_{\Delta d} = \frac{\Delta_{ud}}{\Delta_y} = \frac{2.5}{1.25} = 2$$

$$\xi = 0.05 + \frac{\left(1 - \dfrac{0.95}{\sqrt{2}} - 0.05\sqrt{2}\right)}{\pi} = 0.13$$

From Figure 36.20, find $\Delta_d = 2.45$ in. (62.2 mm) close to $\Delta_{ud} = 2.5$ in. (63.5 mm)   OK
Displacement demand $\Delta_d = 2.45$ in. (62.2 mm).

Discussion

It can be seen that the displacement demand Δ_d of 2.45 in. (62.2 mm) is less than the available ultimate displacement capacity of $\Delta_u = 2.61$ in. (66.3 mm). It should be pointed out that in the actual seismic evaluation of this frame, the flexibility of the steel column to the footing bolted connection should be considered.

References

1. Chen, W. F., *Plasticity in Reinforced Concrete*, McGraw-Hill, New York, NY, 1982.
2. Clough, R. W. and Penzien, J., *Dynamics of Structures*, 2nd ed., McGraw-Hill, New York, 1993.
3. Fung, Y. C., *First Course in Continuum Mechanics*, 3rd ed., Prentice-Hall Engineering, Science & Math, Englewood Cliffs, NJ, 1994.

4. Chen, W. F. and Han, D. J., *Plasticity for Structural Engineers*, Gau Lih Book Co., Ltd., Taipei, Taiwan, 1995.

5. Chopra, A. K., *Dynamics of Structures: Theory and Applications to Earthquake Engineering*, Prentice-Hall, Englewood Cliffs, NJ, 1995.

6. Bathe, K. J., *Finite Element Procedures*, Prentice-Hall Engineering, Science & Math, Englewood Cliffs, NJ, 1996.

7. Priestley, M. J. N., Seible, F., and Calvi, G. M., *Seismic Design and Retrofit of Bridges*, John Wiley & Sons, New York, 1996.

8. Powell, G. H., Concepts and Principles for the Applications of Nonlinear Structural Analysis in Bridge Design, Report No. UCB/SEMM-97/08, Department of Civil Engineering, University of California, Berkeley, 1997.

9. Chen, W. F. and Lui, E. M., *Structural Stability: Theory and Implementation,* Elsevier, New York, 1987.

10. Goto, Y. and Chen, W. F., Second-order elastic analysis for frame design, *J. Struct. Eng. ASCE,* 113(7), 1501, 1987.

11. Allen, H. G. and Bulson, P. S., *Background of Buckling*, McGraw-Hill, London, 1980.

12. White, D. W. and McGuire, W., Method of Analysis in LRFD, Reprints of ASCE Structure Engineering Congress '85, Chicago, 1985.

13. Schilling, C. G. Buckling of one story frames, *AISC Eng. J.*, 2, 49, 1983.

14. Ekhande, S. G., Selvappalam, M., and Madugula, M. K. S., Stability functions for three-dimensional beam-column, *J. Struct. Eng. ASCE,* 115(2), 467, 1989.

15. Orbison, J. G., Nonlinear Static Analysis of Three-dimensional Steel Frames, Department of Structural Engineering, Cornell University, Ithaca, NY, 1982.

16. Yang, Y. B. and McGuire, W., Stiffness matrix for geometric nonlinear analysis, *J. Struct. Eng. ASCE,* 112(4), 853, 1986.

17. Yang, Y. B. and McGuire, W., Joint rotation and geometric nonlinear analysis, *J. Struct. Eng. ASCE,* 112(4), 879, 1986.

18. Hognestad, E., A Study of Combined Bending and Axial Load in Reinforced Concrete Members, University of Illinois Engineering Experimental Station, Bulletin Series No. 399, Nov., Urbana, IL, 1951.

19. Kent, D. C. and Park, R., Flexural members with confined concrete, *J. Struct. Div.* ASCE, 97(ST7), 1969, 1971.

20. Popovics, S. A., Review of stress-strain relationship for concrete, *J. ACI*, 67(3), 234, 1970.

21. Park, R. and Paulay, T., *Reinforced Concrete Structures*, John Wiley & Sons, New York, 1975.

22. Wang, W. C. and Duan, L., The stress-strain relationship for concrete, *J. Taiyuan Inst. Technol.*, 1, 125, 1981.

23. Mander, J. B., Priestley, M. J. N., and Park, R., Theoretical stress-strain model for confined concrete, *J. Struct. Eng. ASCE,* 114(8), 1804, 1988.

24. Mander, J. B., Priestley, M. J. N., and Park, R., Observed stress-strain behavior of confined concrete, *J. Struct. Eng. ASCE,* 114(8), 1827, 1988.

25. Hoshikuma, J., et al., Stress-strain model for confined reinforced concrete in bridge piers, *J. Struct. Eng. ASCE,* 123(5), 624, 1997.

26. William, K. J. and Warnke, E. P., Constitutive model for triaxial behavior of concrete, *Proc. IABSE,* 19, 1, 1975.

27. Mander, J. B., Priestley, M. J. N., and Park, R., Seismic Design of Bridge Piers, Research Report No. 84-2, University of Canterbury, New Zealand, 1984.

28. Chai, Y. H., Priestley, M. J. N., and Seible, F., Flexural Retrofit of Circular Reinforced Bridge Columns by Steel Jacketing, Report No. SSRP-91/05, University of California, San Diego, 1990.

29. Vebe, A. et al., Moment-curvature relations of reinforced concrete slab, *J. Struct. Div. ASCE,* 103(ST3), 515, 1977.

30. Holzer, S. M. et al., SINDER, A Computer Code for General Analysis of Two-Dimensional Reinforced Concrete Structures, AFWL-TR-74-228 Vol. 1, Air Force Weapons Laboratory, Kirtland AFB, NM, 1975.

31. Chen, W. F. and Atsuta, T., *Theory of Beam-Columns*, Vol. 1 and 2, McGraw-Hill, New York, 1977.

32. Bresler, B., Design criteria for reinforced concrete columns under axial load and biaxial bending, *J. ACI*, 32(5), 481, 1960

33. Duan, L. and Chen, W. F., A yield surface equation for doubly symmetrical section, *Struct. Eng.*, 12(2), 114, 1990.

34. King, W. S., White, D. W., and Chen, W. F., Second-order inelastic analysis methods for steel-frame design, *J. Struct. Eng. ASCE,* 118(2), 408, 1992.

35. Levy, R., Joseph, F., and Spillers, W. R., Member stiffness with offset hinges, *J. Struct. Eng. ASCE,* 123(4), 527, 1997.

36. Chen, W. F. and S. Toma, *Advanced Analysis of Steel Frames*, CRC Press, Boca Raton, FL, 1994.

37. Aschheim, M., Moehle, J. P., and Mahin, S. A., Design and Evaluation of Reinforced Concrete Bridges for Seismic Resistance, Report, UCB/EERC-97/04, University of California, Berkeley, 1997.

38. Priestley, N., Myths and Fallacies in Earthquake Engineering — Conflicts between Design and Reality, in *Proceedings of Tom Paulay Symposium — Recent Development in Lateral Force Transfer in Buildings,* University of California, San Diego, 1993.

39. Kowalsky, M. J., Priestley, M. J. N., and MacRae, G. A., Displacement-Based Design, Report No. SSRP-94/16, University of California, San Diego, 1994.

40. Duan, L. and Cooper, T. R., Displacement ductility capacity of reinforced concrete columns, *ACI Concrete Int.*, 17(11). 61, 1995.

41. Akkari, M. M., Nonlinear push-over analysis of reinforced and prestressed concrete frames, *Structure Notes*, State of California, Department of Transportation, Sacramento, July 1993.

42. Akkari, M. M., Nonlinear push-over analysis with p-delta effects, *Structure Notes,* State of California, Department of Transportation, Sacramento, November 1993.

43. MacRae, G. A., Priestly, M. J. N., and Tao, J., P-delta design in seismic regions, Structure System Research Project Report No. SSRP-93/05, University of California, San Diego, 1993.

44. Mahin, S. and Boroschek, R., Influence of geometric nonlinearities on the seismic response and design of bridge structures, *Background Report,* California Department of Transportation, Division of Structures, Sacramento, 1991.

45. Takeda, T., Sozen, M. A., and Nielsen, N. N., Reinforced concrete response to simulated earthquakes, *J. Struct. Div. ASCE,* 96(ST12), 2557, 1970.

46. ADINA, *ADINA-IN for ADINA User's Manual*, ADINA R & D, Inc., Watertown, MA, 1994.